NASA Technical Memorandum 104268

Flow-Visualization Study of the X-29A Aircraft at High Angles of Attack Using a 1/48-Scale Model

Lt. Stacey J. Cotton and Lisa J. Bjarke

August 1994

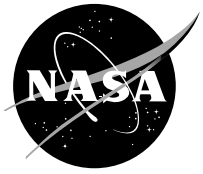

National Aeronautics and
Space Administration

NASA Technical Memorandum 104268

Flow-Visualization Study of the X-29A Aircraft at High Angles of Attack Using a 1/48-Scale Model

Lt. Stacey J. Cotton
USAF

Lisa J. Bjarke
NASA Dryden Flight Research Center
Edwards, California

1994

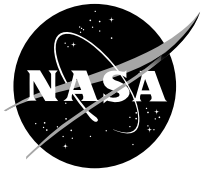

National Aeronautics and
Space Administration

Dryden Flight Research Center
Edwards, California 93523-0273

CONTENTS

ABSTRACT

A water-tunnel study on a 1/48-scale model of the X-29A aircraft was performed at the NASA Dryden Flow Visualization Facility. The water-tunnel test enhanced the results of the X-29A flight tests by providing flow-visualization data for comparison and insights into the aerodynamic characteristics of the aircraft. The model was placed in the water tunnel at angles of attack from 20° to 55° and with angles of sideslip from 0° to 5°. In general, flow-visualization techniques provided useful information on vortex formation, separation, and breakdown and their role in yaw asymmetries and tail buffeting. Asymmetric forebody vortices were observed at angles of attack greater than 30° with 0° sideslip and greater than 20° with 5° sideslip. While the asymmetric flows observed in the water tunnel did not agree fully with the flight data, they did show some of the same trends. In addition, the flow visualization indicated that the interaction of forebody vortices and the wing wake at angles of attack between 20° and 35° may cause vertical-tail buffeting observed in flight.

INTRODUCTION

The NASA Dryden Flight Research Facility began flight testing the X-29A aircraft on December 14 1984. The original tests with the first aircraft covered a flight envelope that went up to Mach 1.48, just above an altitude of 50,000 ft, and up to an angle of attack of 22.5° (ref. 1). On May 23, 1989 the second X-29A made its maiden flight, marking the beginning of the high-angle-of-attack expansion program. The expansion involved tests that attained a maximum transient angle of attack (α) of 67°. The aerodynamic-characterization phase of flight tests with the second X-29A was conducted from July through September 1991. An objective of these flight tests was to inject smoke beneath the nose strake of the aircraft to examine the formation of the off-surface vortices and separated flow over the forebody of the aircraft. Videos and still photographs recorded during flight provided valuable insight into the formation, separation, and breakdown of vortices.

Interesting results from these flight tests showed that at zero sideslip ($\beta = 0°$) yaw asymmetries develop above $\alpha = 40°$ (refs. 2–4). Above $\alpha = 40°$ the body axis yawing moment, C_{n_0}, becomes positive and reaches a maximum at $\alpha = 45°$. From $\alpha = 45°$ to 48° C_{n_0} is decreasing but still positive. The yaw asymmetry transitions from positive to negative at $\alpha = 48°$, and C_{n_0} becomes increasingly negative as α is increased up to 55°. The presence of strong asymmetric forebody vortices at these high angles of attack may explain the yaw asymmetry. Wind-tunnel tests conducted at NASA Langley Research Center show that above $\alpha = 25°$ to 30°, the forebody design is the most dominant configuration feature affecting the flow field (ref. 5). Another possible vortex-related phenomenon is the tail buffeting that begins at $\alpha = 20°$ and peaks at $\alpha = 30°$.[1]

To gain insight to the flight results, a water-tunnel test was conducted at the NASA Dryden Flow Visualization Facility. The water-tunnel test showed the flow phenomena that caused the yawing moments and tail buffeting measured in flight. In addition, the results from this study provided a flow-visualization database on the high-angle-of-attack characteristics of the X-29A.

The NASA Dryden water tunnel provides an excellent opportunity for viewing the formation of vortices and separated flow at high angles of attack. The low flow rates attained in the water tunnel result in lower Reynolds numbers than those generated in flight. However, high-angle-of-attack flow fields that exhibit separation everywhere along the leading edge of the wing and are vortex dominated can be well-simulated in a low Reynolds number-generating water tunnel (ref. 6). At the stall angle of attack, sharp leading edges exhibit an adverse pressure gradient

[1]Ryan, Robert, "X-29 Structural Load Results From the High Alpha ⁄ 0.60 Mach Envelope Expansion," Grumman Aircraft Systems Interoffice Memorandum, 30 Aug. 1990 (copy available from author of this paper).

that causes the flow to separate. Because the gradient is so adverse, it is likely to trip the flow for a range of Reynolds numbers. Thus, when leading-edge separation occurs, the flow field is less Reynolds number dependent. At high angles of attack, the X-29A exhibits vortex-dominated flow and separation at the leading edge of the wing, and thus the use of the water tunnel was considered appropriate for this study.

The water-tunnel test was modeled after the aerodynamic-characterization flight test (ref. 7). The angles of attack were varied from $\alpha = 20°$ to 55°. Sideslip angle was varied from $\beta = 0°$ to 5°. Canard settings were based on simulation data for the aircraft flying at 15,000 ft and at Mach 0.2.

APPARATUS AND PROCEDURE

Flow Visualization Facility

The NASA Dryden Flow Visualization Facility is a single-return water tunnel with a 24- by 16- by 72-in. test section. Figure 1 shows a schematic of the water tunnel. The walls are made of 2-in. thick transparent acrylic plastic. The velocity of the water can be varied from 0 to 13.5 in./sec. This test was conducted at 3.0 in./sec because of the dye-stream clarity at this velocity. The model was sting mounted. The angle of attack, angle of sideslip, and canard angle could be varied independently during the test.

Model Description

The study used a 1/48-scale model constructed at the NASA Dryden Flow Visualization Facility. The model was a brass frame covered with machinable filler paste that comprised the skin. Inlet flow was simulated by extracting water through the inlet and out a tube at the base of the model. Flow meters regulated the flow and simulated flight engine mass flow.

Dye ports placed at various locations on the model provided flow visualization. Figures 2(a) and 2(b) show the locations of the various dye ports. The dye tubes originated from an external source, were fed through the interior of the model, and terminated at the ports.

The model had internal dye lines with ports on the forebody, canards, and wings. Additional external dye lines were added later on the engine inlets and the leading edge of the vertical tail. The purpose of the engine-inlet dye ports was to determine if the flow over the engine inlets was affecting the character of the forebody vortices. The vertical-tail dye ports served to determine the character of the flow field in the region of the vertical tail.

Test Conditions

The water tunnel was operated at a flow velocity of 3.0 in./sec, corresponding to a unit Reynolds number of 2.5×10^4/ft. The average temperature of the water was 75° F.

The test was videotaped and photographed using 120-mm film. The still photographs recorded side and front views between $\alpha = 20°$ to 55° and at $\beta = 0°$ and 5°. The videotape provided additional data for detailed analysis of the dynamics and stability of the flow field around the fuselage.

The canard deflection schedule for the X-29A aircraft used in the water-tunnel tests is shown in Fig. 3 as canard angle versus angle of attack. Wing flaps were fixed at 20°, trailing edge down.

RESULTS AND DISCUSSION

The angle of attack of the X-29A model was varied from 20° to 55° at sideslip angles of 0° and 5°. At $\alpha = 20°$, forebody vortices formed at the nose strakes, which have sharp leading edges. Therefore, it is assumed that the general character of the forebody vortices above $\alpha = 20°$ will not be highly Reynolds number dependent (ref. 6).

In the results presented, vortices are described in terms of strength, breakdown point, and separation point. In general, the strength of a vortex is characterized by the tightness of the core and the number of revolutions per distance along the core. The stronger vortex will always have more revolutions per distance and may have a tighter core. The results are qualitative and therefore vortex strength in terms of number of revolutions per distance is not measured, but determined by observation. The breakdown point is that location at which the core of the vortex is diffused and the fluid motion irregular. Finally, the separation point of the vortex refers to the location at which a vortex that has been attached to the fuselage leaves the surface. After the separation point, the vortex path may flow over the fuselage at a given distance or sometimes flow into the free stream.

Sideslip Configuration, $\beta = 0°$

At $\alpha = 20°$ (fig. 4), two symmetric weak forebody vortices form and flow down the fuselage along the left and right side of the canopy. These vortices separate from the fuselage as they approach the canopy, travel past the canopy on either side, and then follow the fuselage closely again aft of the canopy until breakdown, which occurs at a point even with the inboard corner of the flap hinge line. Leading edge flow separation occurs on both the canards and wings.

At $\alpha = 25°$ (fig. 5), the breakdown point of the two symmetric forebody vortices has moved farther forward along the fuselage than at $\alpha = 20°$ (fig. 4). This breakdown is nearer the canopy, at a point even with the trailing edge of the wingtip. The forebody vortices break down as they approach the surface of the fuselage (fig. 5(b)). A left wingtip vortex flows into the free stream (fig. 5(a)). Weak canard vortices form along the leading edge and travel outboard to form a weak canard tip vortex.

At $\alpha = 30°$ (fig. 6), a small amount of asymmetry is seen in the forebody vortex paths aft of the canopy. The left forebody vortex follows the fuselage more closely than the right forebody vortex. The breakdown point of the forebody vortices has not changed from that at $\alpha = 25°$. The canard vortices are stronger, with a tighter core, and flow into the free stream where they break down at a point even with the leading edge of the vertical tail. Left and right symmetric wingtip vortices now appear.

At $\alpha = 35°$ (fig. 7), the asymmetry in the forebody vortex paths is more apparent with the left forebody vortex staying nearer the fuselage aft of the canopy. In addition, the left forebody vortex breaks down before the right forebody vortex, just aft of a point even with the trailing edge of the canard (fig. 7(a)). The canard tip vortices are stronger, but the turbulence behind the forebody vortex breakdown appears to cause the canard tip vortex breakdown to occur farther forward than at $\alpha = 30°$ (fig. 6). No wingtip vortices appear at $\alpha = 35°$.

At $\alpha = 40°$ (fig. 8), the forebody vortices are stronger and the asymmetry more pronounced than at $\alpha = 35°$ (fig. 7). The left forebody vortex stays nearer the fuselage and breaks down farther forward than the right vortex. The right forebody vortex breaks down as it passes the top of the vertical tail (fig. 8(b)). The breakdown point of the left forebody vortex is unchanged between $\alpha = 35°$ and 40°. The canard tip vortices are stronger at $\alpha = 40°$ than at 35°. The breakdown of the right canard tip vortex occurs farther forward than that of the left. The left canard tip vortex breaks down as it passes outboard of the leading edge of the vertical tail.

At $\alpha = 45°$ (fig. 9), the forebody vortices are stronger than at $\alpha = 40°$ (fig. 8), and the right forebody vortex flows into the free stream and breaks down far aft of the model. The left forebody vortex is nearer the top of the fuselage and breaks down farther forward, over the centering of the fuselage, even with the trailing edge of the canard tip. The strength of the canard tip vortices is similar to that at $\alpha = 40°$, but the breakdown point of the left vortex is farther forward and breaks down over the trailing edge of the left wing. The breakdown point of the right canard tip vortex has not changed from that at $\alpha = 40°$.

At $\alpha = 50°$ (fig. 10), the vortex asymmetry on the forebody switches from the strong, dominant right forebody vortex shown at $\alpha = 45°$ (fig. 9) to a strong left forebody vortex. At this angle of attack, the left forebody vortex separates from the forebody forward of the canopy, moves outboard, and passes above and to the left of the vertical tail and strake flaps. The left forebody vortex extends past the base of the aircraft into the free-stream flow. The right forebody vortex, however, remains near the forebody, travels to the left over the canopy and vortex core breakdown occurs at the trailing edge of the right canard. Both canard tip vortices are weaker than at $\alpha = 45°$. The stronger left forebody vortex may initiate the breakdown of the left canard vortex, since the two vortices tend to converge as they progress into the free-stream flow.

At $\alpha = 55°$ (fig. 11), the flow along the forebody is turbulent, and the paths of the two forebody vortices appear symmetric. However, the forebody vortices appear asymmetric in breakdown, with the left vortex breaking down before it passes over the canopy and the right vortex breaking down directly over the canopy. The canard tip vortices are much weaker than at $\alpha = 50°$ (fig. 10) and break down almost immediately.

Sideslip Configuration, $\beta = 5°$

At $\alpha = 20°$ (fig. 12), the flow field on the wings and canards is completely separated. This configuration reveals a weak leeward forebody vortex. The leeward forebody vortex (black dye) (fig. 12(b)), forms at the nose strake and flows along the left side of the fuselage, where it breaks down as it passes the left-engine inlet. The windward forebody flow (red dye) comes from underneath the nose, travels around the fuselage over the canopy, and separates at the aft end of the canopy.

At $\alpha = 25°$ (fig. 13) and $\alpha = 30°$ (fig. 14), the flow fields are similar with only slight variations in the location of forebody vortices and canard tip vortex strength. At $\alpha = 25°$, the leeward nose-strake vortex is stronger than at $\alpha = 20°$ (fig. 12); it flows over the top of the left engine inlet and breaks down at the midpoint of the left-wing root. The windward flow moves from the side of the fuselage to the top at a point farther forward than that at $\alpha = 20°$. A left-wingtip vortex appears at $\alpha = 25°$. At $\alpha = 30°$, the breakdown point of the leeward nose-strake vortex has moved farther aft and now breaks down even with the flap hinge line of the left wing. The windward flow (a weak forebody vortex), crosses over the centerline of the canopy. A weak leeward canard vortex breaks down as it passes over the left wing. In comparing the flow fields at these angles of attack for sideslip angles of 0° and 5°, it is evident that the sideslip creates a tendency for the leeward forebody vortex to be stronger than the windward forebody vortex. For 0° sideslip at these angles of attack (figs. 5 and 6), the strength of the forebody vortices is about the same on both sides of the aircraft.

At $\alpha = 35°$ (fig. 15) and $\alpha = 40°$ (fig. 16), the flow fields are also similar with only slight variations. At $\alpha = 35°$, the leeward forebody vortex flows above the fuselage along the leeward side and breaks down at a point slightly forward but outboard of the base of the vertical tail (fig. 15(a)). The windward forebody vortex has increased in strength from $\alpha = 30°$ (fig. 14), and the breakdown point has moved farther aft and outboard along the top of the fuselage. Tip vortices can be seen on both canards and both wings. The leeward canard vortex breaks down over the left wing. At $\alpha = 40°$, the leeward forebody vortex is stronger than at $\alpha = 35°$, and in the region between the canopy and vertical tail, the vortex path is higher off the surface (fig. 15(b)). Flow from underneath the nose strake and underneath

the windward side of the aircraft now combines (black and red dye) to form the windward forebody vortex. The windward forebody vortex is stronger than at $\alpha = 35°$, but breakdown occurs sooner, over the canopy. The leeward canard tip vortex appears to break down farther aft than at $\alpha = 35°$. The two wingtip vortices have decreased in strength from $\alpha = 35°$ and break down just aft of each trailing edge. A comparison of the flow fields for $\alpha = 35°$ and 40° at $\beta = 0°$ and 5° shows that with zero sideslip (figs. 7 and 8), the forebody vortices tend to be stronger in terms of number of revolutions per distance. In general, with sideslip added, the results at these angles of attack reveal that the windward canard vortex is stronger than the leeward canard vortex and that the leeward forebody vortex is stronger than the windward forebody vortex.

At $\alpha = 45°$ (fig. 17), the leeward forebody vortex is stronger than at $\alpha = 40°$ (fig. 16), but breaks down farther forward, just aft of the canopy. The windward forebody vortex is stronger than at $\alpha = 40°$, with a tighter core, but the breakdown point is unchanged. The leeward canard vortex is much weaker than at $\alpha = 40°$ and breaks down just aft of the canard trailing edge. The windward canard tip vortex does not flow in the direction of the free stream, as it does at $\alpha = 40°$ and below; instead it tends to flow toward the leeward side of the aircraft, over the vertical tail.

At $\alpha = 50°$ (fig. 18), the leeward forebody vortex is stronger than at $\alpha = 45°$ (fig. 17) and flows into the free stream where it breaks down aft of the model. Separate nose-strake and forebody vortices are on the windward side of the model. The nose-strake vortex forms underneath the nose strake on the windward side (black dye) and flows over the center of the fuselage, where it breaks down approaching the canopy. The windward forebody vortex (red dye) forms underneath the windward side of the aircraft and flows over the canopy onto the leeward side, where it breaks down passing over the leeward engine inlet. At $\alpha = 50°$, the canard vortices both break down near the leading edge of the wing, whereas at $\alpha = 45°$ the canard vortex breakdown is asymmetric. A comparison at $\alpha = 50°$ for $\beta = 0°$ and 5° shows that the character of the forebody vortices is similar for both cases, with the zero-sideslip forebody vortices (fig. 10) being stronger.

At $\alpha = 55°$ (fig. 19), the nose-strake vortices (black dye) are stronger and the canard tip vortices are weaker than at $\alpha = 50°$ (fig. 18). The windward forebody vortex (red dye) is much weaker at this angle of attack and breaks down as it approaches the canopy. The leeward forebody vortex flows into the free stream and breaks down far aft of the model. The windward nose-strake vortex (black dye) separates from the fuselage at the canopy and flows above the fuselage until it breaks down above the canard. At $\alpha = 55°$ and $\beta = 5°$, the forebody vortices are asymmetric; while at zero sideslip (fig. 11) the forebody vortices are symmetric.

Correlation of Flow-Field Characteristics and Yaw Asymmetries

As stated previously, yaw asymmetries were noted during the high angle-of-attack envelope expansion phase of flight tests between $\alpha = 30°$ and 55° (fig. 20). During the water-tunnel tests, asymmetries also were noted in the forebody vortices for this angle-of-attack range. The following discussion will examine the cause of the forebody vortex asymmetry seen in the water tunnel and the correlation with yaw asymmetries experienced in flight.

First, it appears that the nose strakes have a profound impact on the formation of the forebody vortices. During preliminary runs on the model, a small amount of filler paste was discovered on one of the nose strakes. When the paste was removed, the character of the forebody vortices was changed completely.

In addition to the nose strakes, the effect of the engine inlets on the forebody vortices was investigated. The results of the tests show that weak vortices formed at the top of the engine inlets. However, the forebody vortices were much stronger than the engine-inlet vortices, and thus they did not appear to be affected by the vortices on the engine inlets.

As noted in a previous section, the zero-sideslip forebody vortex asymmetry first appears at $\alpha = 30°$ and increases to a maximum at $\alpha = 45°$. This asymmetry is characterized by the right vortex path traveling into the free stream and breaking down aft of the model while the left forebody vortex follows closely along the fuselage and breaks down behind the canopy ($\alpha = 45°$, fig. 9). At $\alpha = 50°$ (fig. 10), this asymmetry is reversed; the left vortex follows the free stream breaking down far aft of the model while the right follows the fuselage more closely and breaks down over the trailing edge of the right canard. At $\alpha = 55°$ (fig. 11), the forebody flow field is turbulent, but the forebody vortex paths appear symmetric. These trends are summarized qualitatively in Fig. 20.

The forces resulting from these vortex asymmetries could not be measured in the water tunnel. However, in cases ($\alpha = 35°$ to 40°) where the left forebody vortex is nearer the fuselage than the right, the pressure near the fuselage seems lower on the left side than the right, causing a nose-left yawing moment. Conversely at $\alpha = 50°$, when the right forebody vortex is nearer the fuselage than the left, a nose-right yawing moment would result. Thus, asymmetry in the path and breakdown of the forebody vortices may cause asymmetric yawing moments.

Although the data shown in Fig. 21 reveal that the in-flight yaw asymmetry is the opposite from that obtained in the water tunnel, slight variations are likely in the geometry of the model forebody and the actual aircraft forebody. Such slight geometric variations may be enough to establish the asymmetry in forebody vortices at the farthest forward portion of the forebody. Thus, although the forebody vortex asymmetry results from the water tunnel do not coincide directly with the in-flight results, they reveal that the cause of the asymmetric forebody vortices may be the sensitive forward portion of the forebody and particularly the nose strake.

Angle-of-Attack Range for Known Tail Buffeting

In-flight tail buffeting has been observed to start at $\alpha = 20°$. The maximum buffet activity occurs at $\alpha = 30°$ and then dissipates as the angle is increased to $\alpha = 35°$ (footnote, p. 1). The angle of attack on the X-29A model was varied from 20° to 35° at zero sideslip to examine the effects of the flow field on the vertical tail.

Water-tunnel results show interaction of the wing wake and the forebody vortices in the angle-of-attack range for known tail buffeting. The wing wake tends to collide with the forebody vortices trailing along the sides of the fuselage. From an analysis of the video, the flow behind the wings rotates clockwise behind the right wing and counterclockwise behind the left wing, as seen looking from the tail toward the nose. This inboard-moving flow is probably a result of the forward swept wing geometry (ref. 7). The forebody vortices each rotate outboard, in a direction opposite to the flow behind the wing. From $\alpha = 20°$ to 35°, the forebody vortices and the rotating wing wake collide in the region near the vertical tail (figs. 4–7). The flow around the vertical tail exhibits a low-frequency pulsing motion caused by these colliding flows. Increasing or decreasing the dynamic pressure and Reynolds number would tend to increase or decrease the frequency of pulsing and the force on the vertical tail correspondingly. Depending on these conditions, the interaction of the forebody vortices and wing wake may create varied frequencies and forces on the vertical tail. Thus a correlation could be made with flight conditions that exhibit higher dynamic pressures and Reynolds numbers and the conditions observed in the water tunnel. Figure 6 shows the flow field around the vertical tail at zero sideslip and $\alpha = 30°$.

The strength of the forebody vortices and the location of the flow near the vertical tail also appear to play an important role in vertical-tail buffeting. At $\alpha = 20°$ (fig. 4), weak forebody vortices form. As the angle of attack is increased the forebody vortices increase in strength. In the region between $\alpha = 20°$ and 35° (figs. 4–7), the flow field interacts with the vertical tail. However, as angle of attack increases above 35° (figs. 8–11), the flow field no longer interacts with the vertical tail. Thus it is concluded that the in-flight vertical-tail buffeting observed between $\alpha = 20°$ and 35° is caused by the interaction of the forebody vortices and the wing wake.

The effect of sideslip on the flow field around the vertical tail was also examined. As sideslip is increased, the windward forebody and canard vortex tend to move toward the leeward side of the aircraft. At $\alpha = 30°$ and $\beta = 5°$ (fig. 14), the flow from the broken down windward forebody vortex flows directly into the vertical tail, and the turbulent flow created by the windward canard impinges on the vertical tail. These results show that in the case of sideslip the windward forebody vortex and the turbulent flow field created at the windward canard interacts with the vertical tail in the tail-buffeting angle-of-attack range.

CONCLUDING REMARKS

A water-tunnel study was conducted on a 1/48-scale model of the X-29A aircraft to examine high-angle-of-attack characteristics. Research focused on recording a database of flow characteristics for a range of angles of attack (α) and sideslip (β) while examining possible causes of yaw asymmetry and vertical tail buffeting. The angles of attack ranged between 20° and 55°, while sideslip was varied between 0° and 5°. Results were presented on the general characteristics of the flow, yaw asymmetry, and vertical-tail buffeting.

The yaw asymmetry study shows that forebody vortex path and breakdown asymmetries are seen in the water tunnel in the same angle-of-attack range as the asymmetric yawing moments observed in flight. Moreover, it is likely that the asymmetry in forebody vortices is caused by slight variations at the forward portion of the forebody, specifically at the nose strake. This asymmetry in forebody vortices seen at zero sideslip began at $\alpha = 30°$ with the right forebody vortex stronger and farther off the surface than the left forebody vortex. The asymmetry increased up to $\alpha = 45°$, at which point the asymmetry switched at $\alpha = 50°$ and the left forebody vortex was stronger and farther off the surface. The forebody vortices remained asymmetric up to $\alpha = 55°$, at which point the flow field became turbulent and the forebody vortices appeared symmetric.

Asymmetry in forebody and canard vortices was also seen when sideslip was added. For $\beta = 5°$, the asymmetry in the path and breakdown of forebody vortices began at $\alpha = 20°$, as opposed to $\alpha = 30°$ with zero sideslip, with the formation of one leeward forebody vortex. As the angle of attack was increased, this leeward forebody vortex increased in strength, until at $\alpha = 50°$ it flowed into the free stream. A weaker windward forebody vortex formed at $\alpha = 30°$ and a windward nose-strake vortex formed at $\alpha = 50°$. These windward vortices were always weaker than the dominant leeward forebody vortex.

For $\beta = 5°$, a weak leeward canard vortex forms at $\alpha = 30°$; but as the angle of attack is increased, the windward canard vortex dominates and the leeward canard vortex breaks down sooner. Asymmetry in the breakdown point of canard vortices was seen in both 0° and 5° sideslip cases. For zero sideslip, the strong asymmetry in the forebody vortices appeared to play a large role in determining the breakdown point of the canard vortices. When sideslip was added, the windward canard vortex and the leeward forebody vortex dominated.

The results from the vertical-tail buffeting study reveal that the interaction of the wing wake and the forebody vortices in the $\alpha = 20°$ to 35° range correlates with in-flight vertical-tail buffeting. The collision between the forebody vortices and the wing wake creates a pulsing motion of the flow in the region of the vertical tail. In addition, the wake from the windward forebody and the turbulent flow from the windward canard at $\alpha = 30°$ and $\beta = 5°$ impinge on the vertical tail. At higher dynamic pressures and Reynolds numbers such as those seen in flight, the interaction of the forebody vortices, wing wake, and canard flow in the region of the vertical tail may create the frequency and forces exhibited during in-flight tail buffeting.

Dryden Flight Research Facility
National Aeronautics and Space Administration
Edwards, California, May 19, 1993

REFERENCES

1. Clarke, Robert, John Burken, Jeffrey Bauer, Michael Earls, Donna Knighton, David McBride, and Fred Webster, *Development and Flight Test of the X-29A High Angle-of-Attack Flight Control System*, NASA TM-101738, Feb. 1991.

2. Webster, Frederick R., Mark A. Croom, and Robert Curry, "Correlation of Ground-Based and Full-Scale Flight Results on Aerodynamics and Flight Dynamics of the X-29," (ITAR limited) in *High-Angle-of-Attack Technology*, Vol. 1, Part 1, pp. 279–303, May 1992.

3. Webster, Frederick R. and Dana Purifoy, "X-29 High Angle-of-Attack Flying Qualities," AFFTCTR-91-15, June 1991, available from Air Force Flight Test Center, Edwards, CA.

4. Pellicano, Paul, Joseph Krumenacker, and David Vanhoy, "X-29 High Angle of Attack Flight Test Procedures, Results, and Lessons Learned," in *Proceedings of the Society of Flight Test Engineers 21st Annual Symposium*, Garden Grove, CA, Aug. 1990, pp. 2.4-1 to 2.4-24.

5. Grafton, S.B., W.P. Gilbert, M.A. Croom, and D.G. Murri, "High Angle of Attack Characteristics of a Forward Swept Wing Fighter Configuration," AIAA-82-1322, Aug. 1982.

6. Erickson, Gary E., "Vortex Flow Correlation," AFWAL-TR-80-3143, USAF Wright Aeronautical Laboratory, Jan. 1981.

7. Del Frate, John H. and John A. Saltzman, *In-Flight Flow Visualization Results from the X-29A Aircraft at High Angles of Attack*, NASA TM-4430, Nov. 1992.

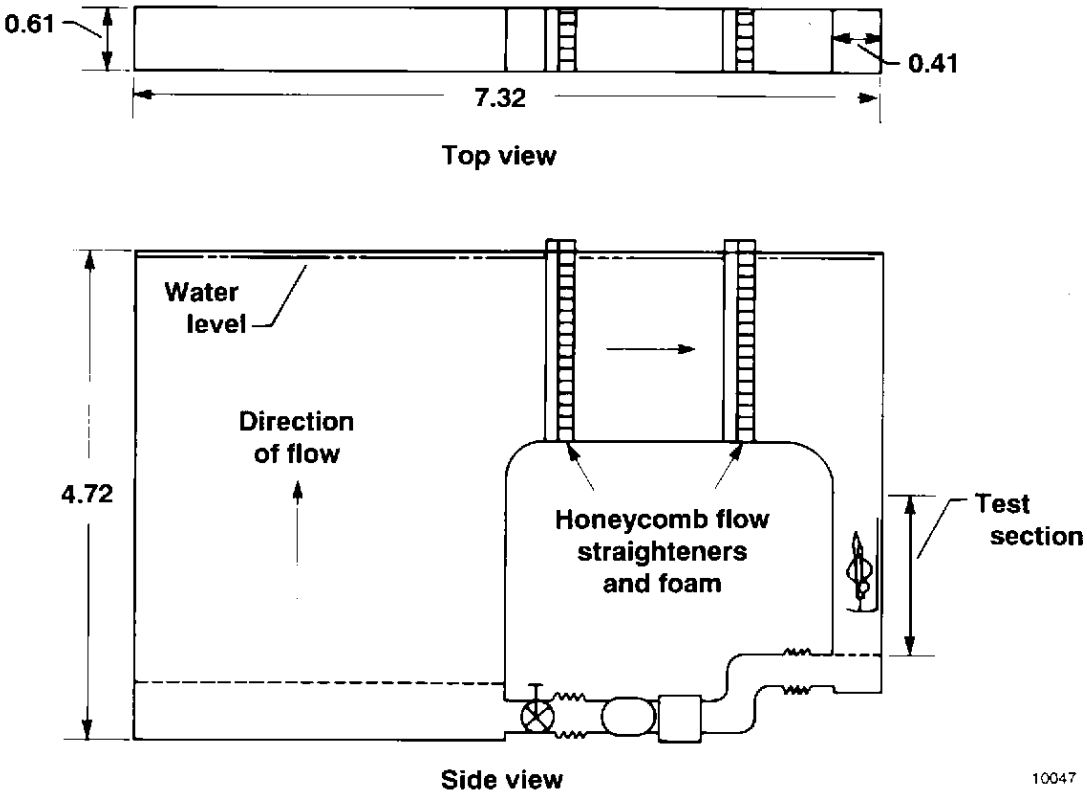

Figure 1. Schematic of NASA Dryden flow visualization system (units in meters).

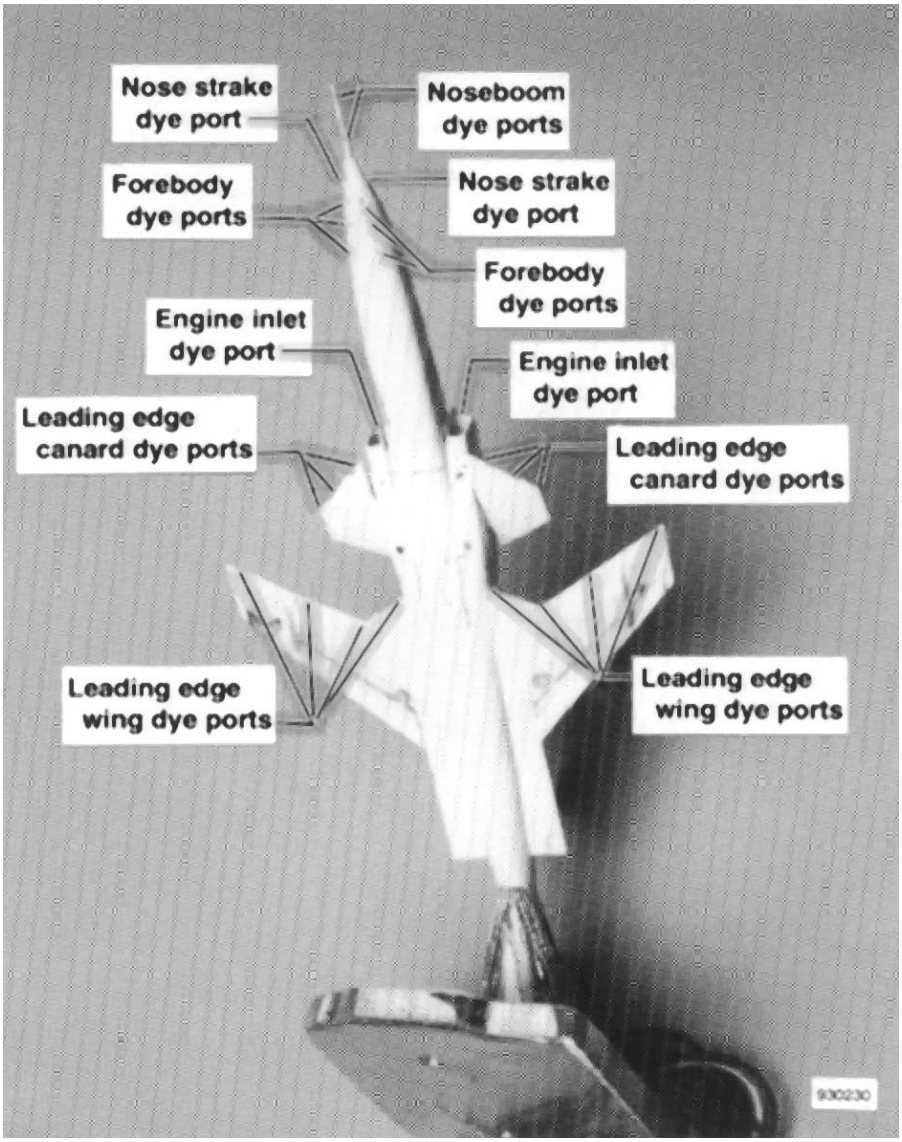

(a) Bottom view.

Figure 2. Scale (1/48) model of X-29A used in water tunnel.

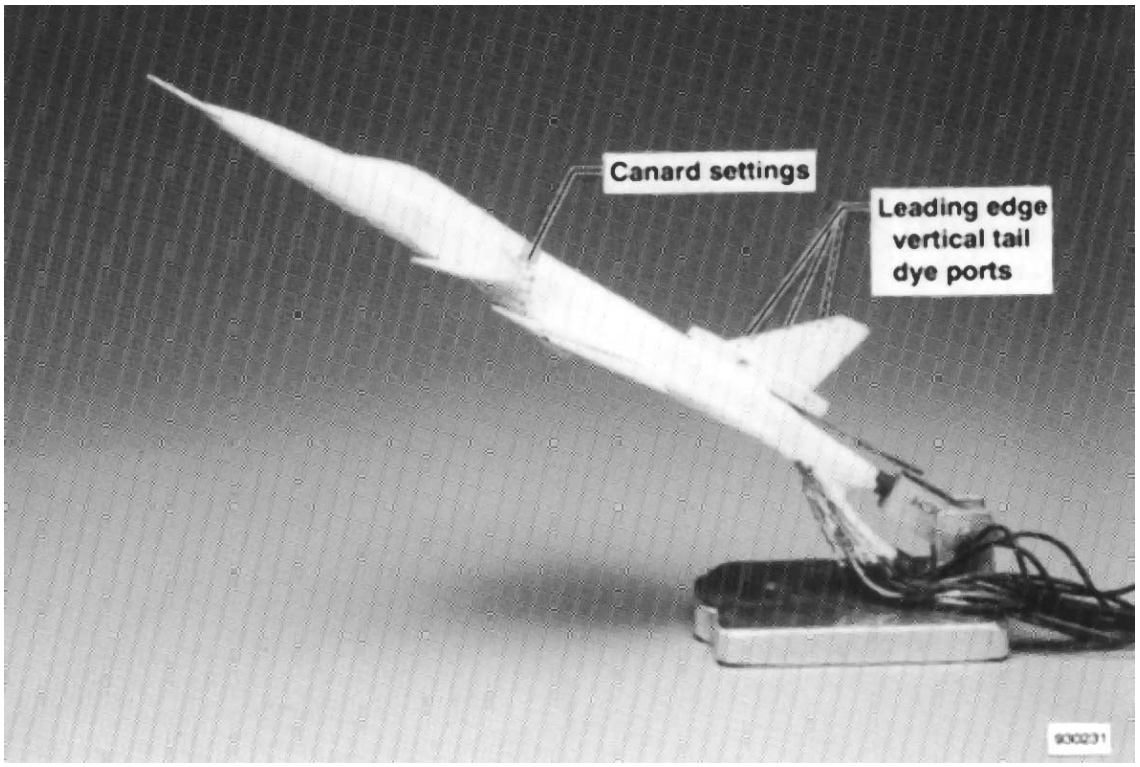

(b) Side view.

Figure 2. Concluded.

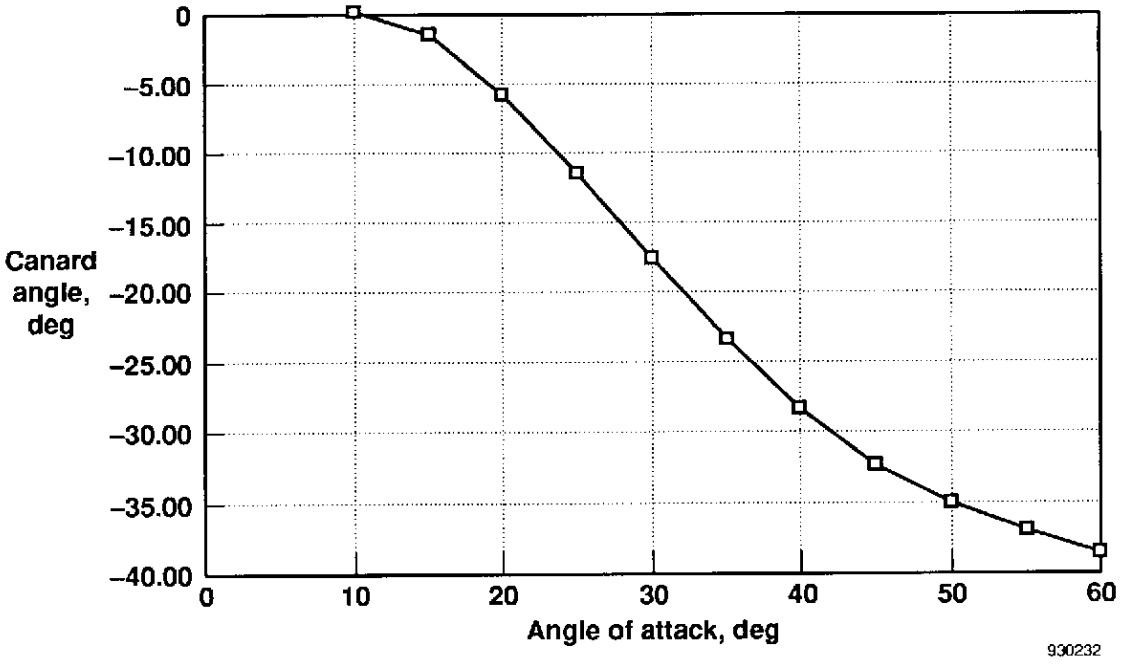

Figure 3. X-29A canard schedule; Mach 0.2 at 15,000 ft.

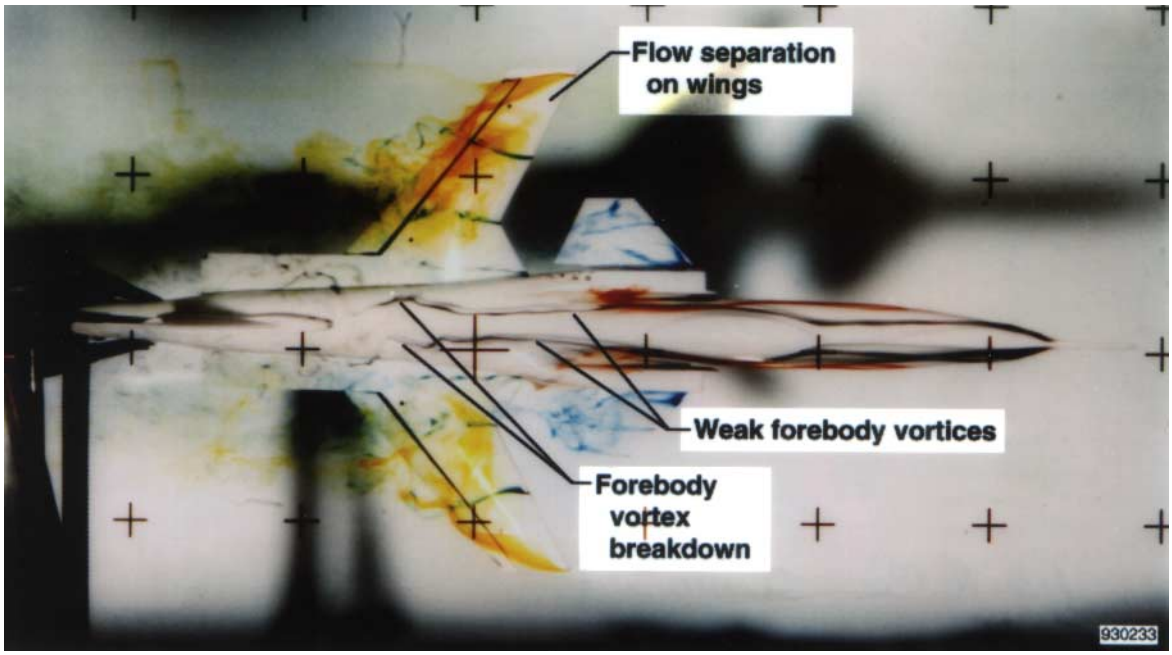

(a) Top view.

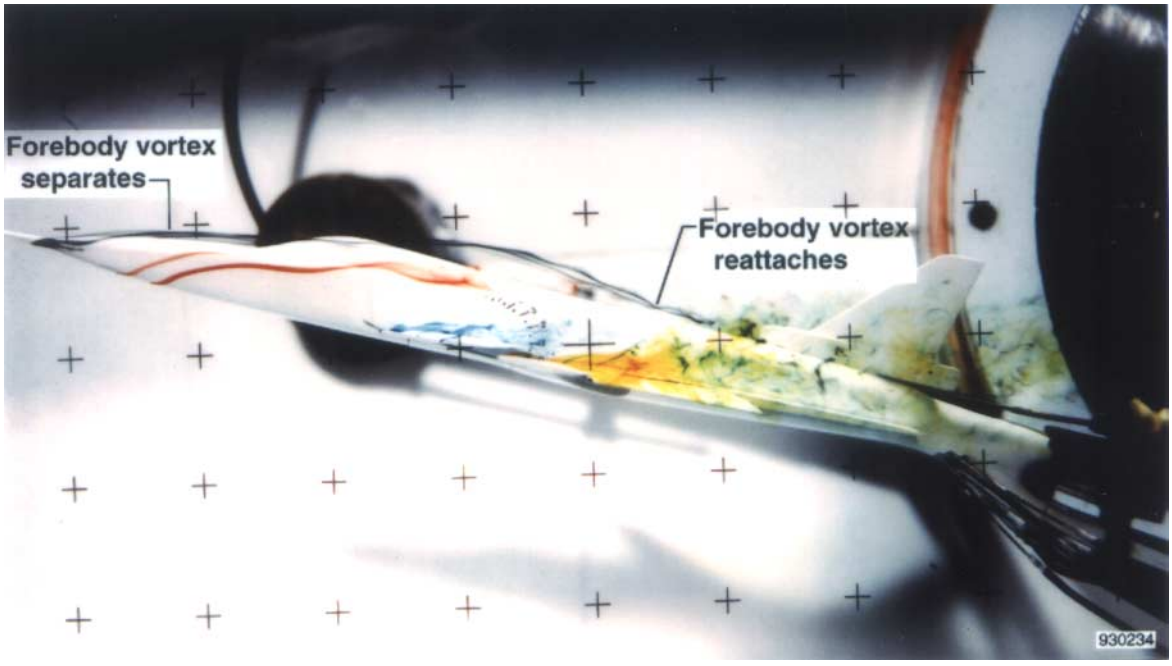

(b) Side view.

Figure 4. Characteristic flow patterns at $\alpha = 20°$ and $\beta = 0°$.

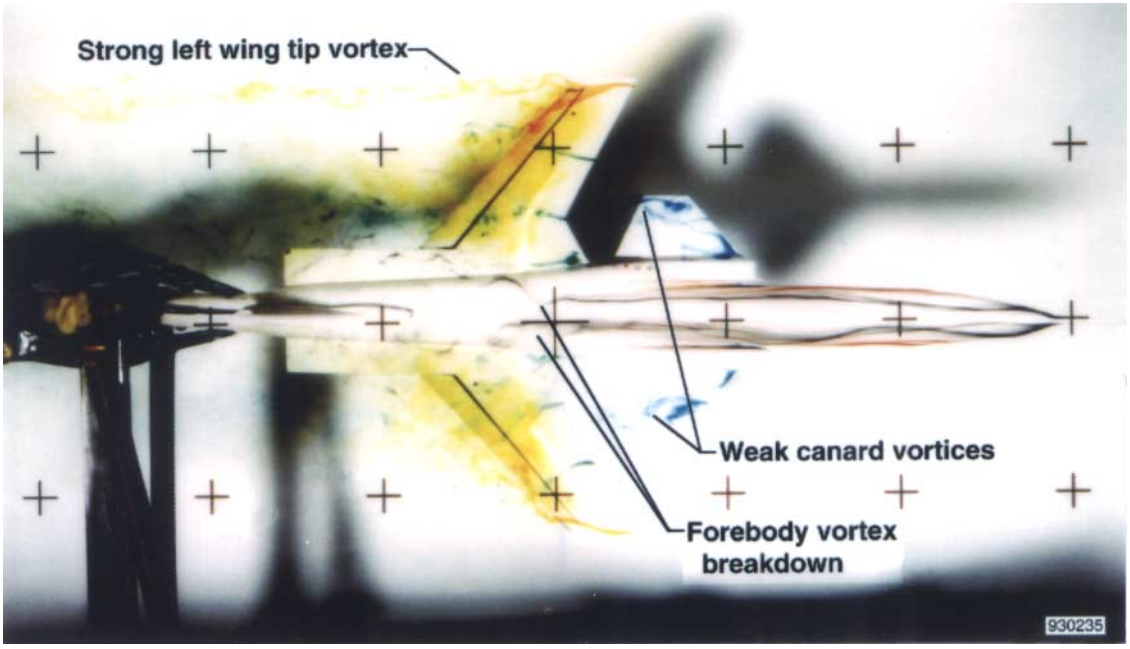

(a) Top view.

(b) Side view.

Figure 5. Characteristic flow patterns at $\alpha = 25°$ and $\beta = 0°$.

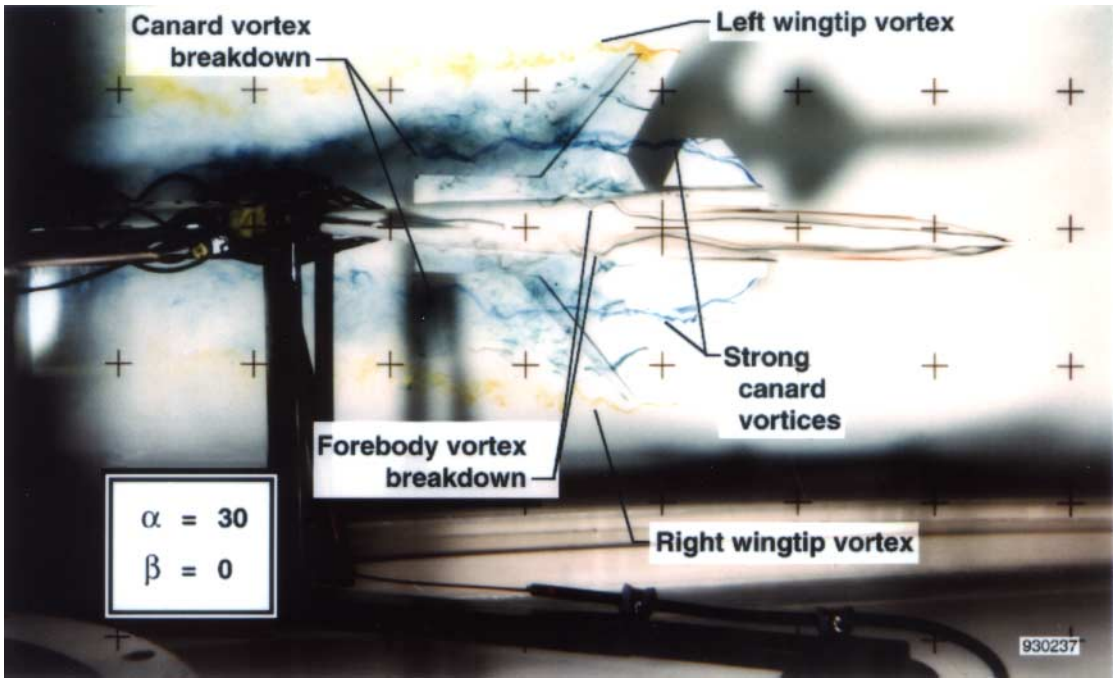

(a) Top view.

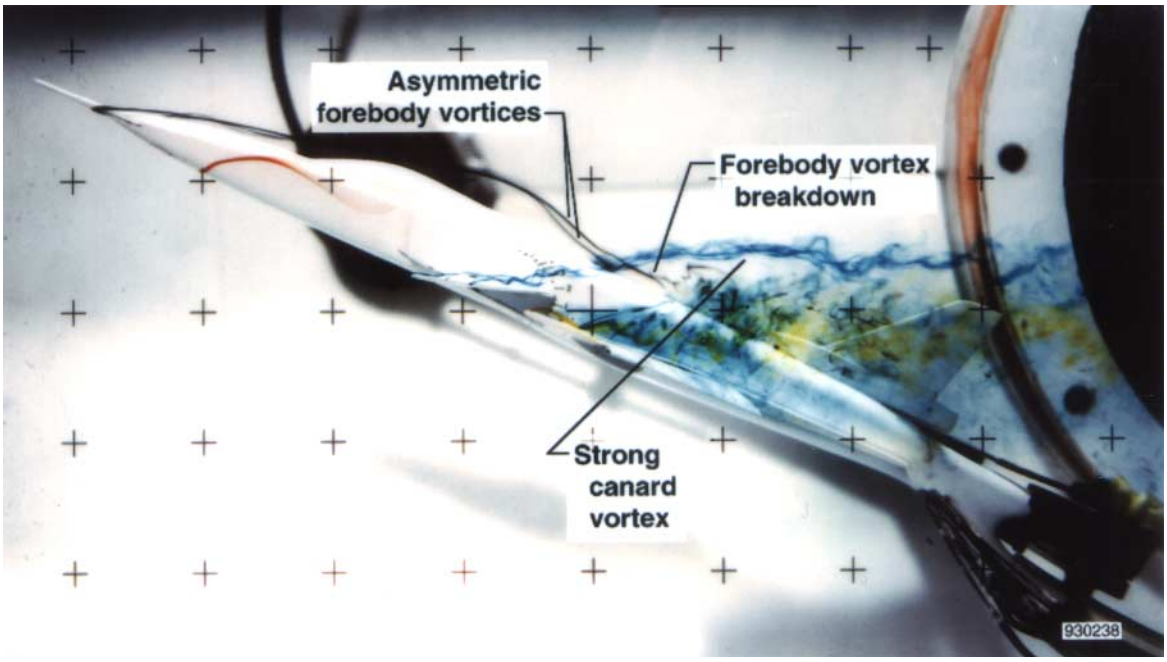

(b) Side view.

Figure 6. Characteristic flow patterns at $\alpha = 30°$ and $\beta = 0°$.

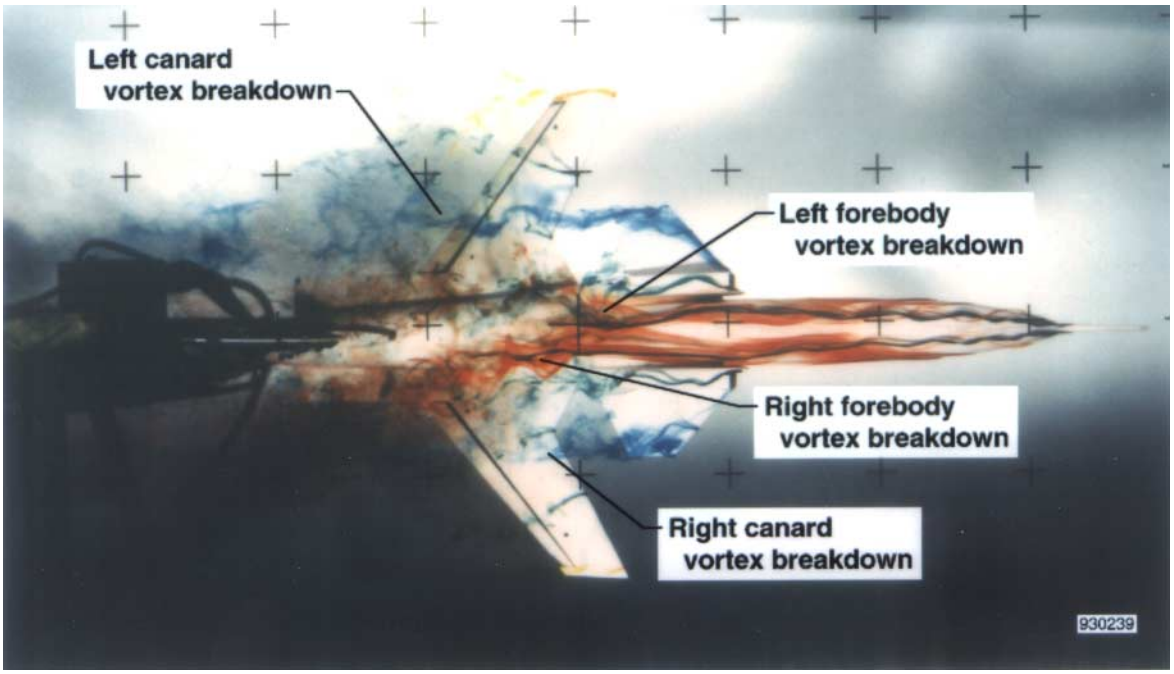

(a) Top view.

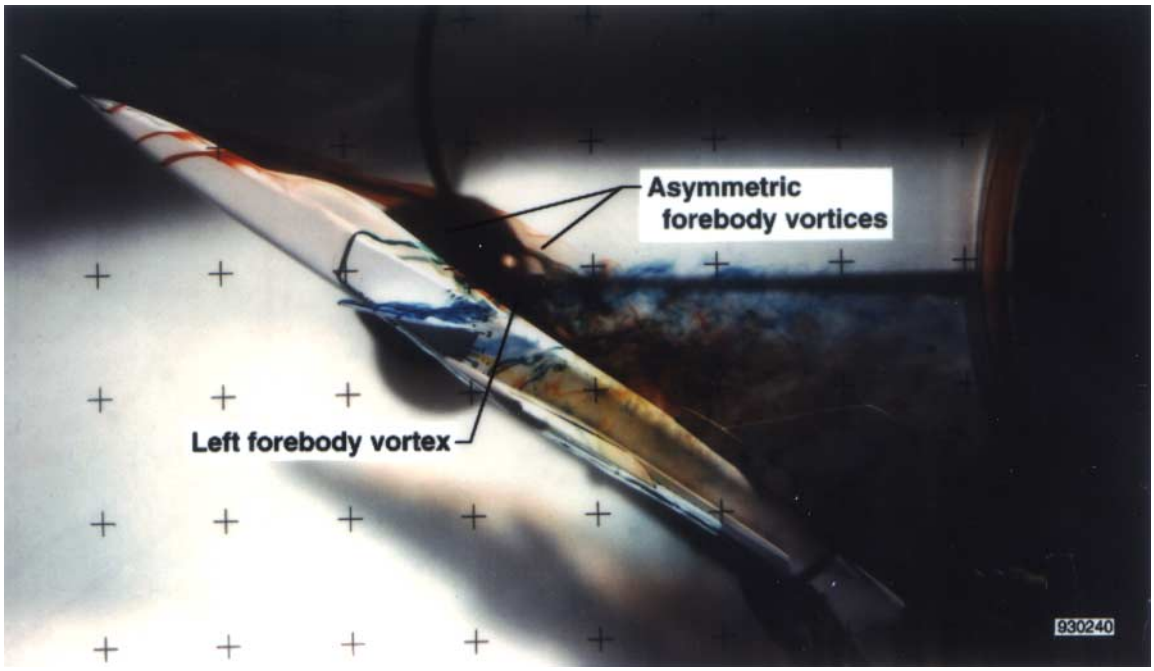

(b) Side view.

Figure 7. Characteristic flow patterns at $\alpha = 35°$ and $\beta = 0°$.

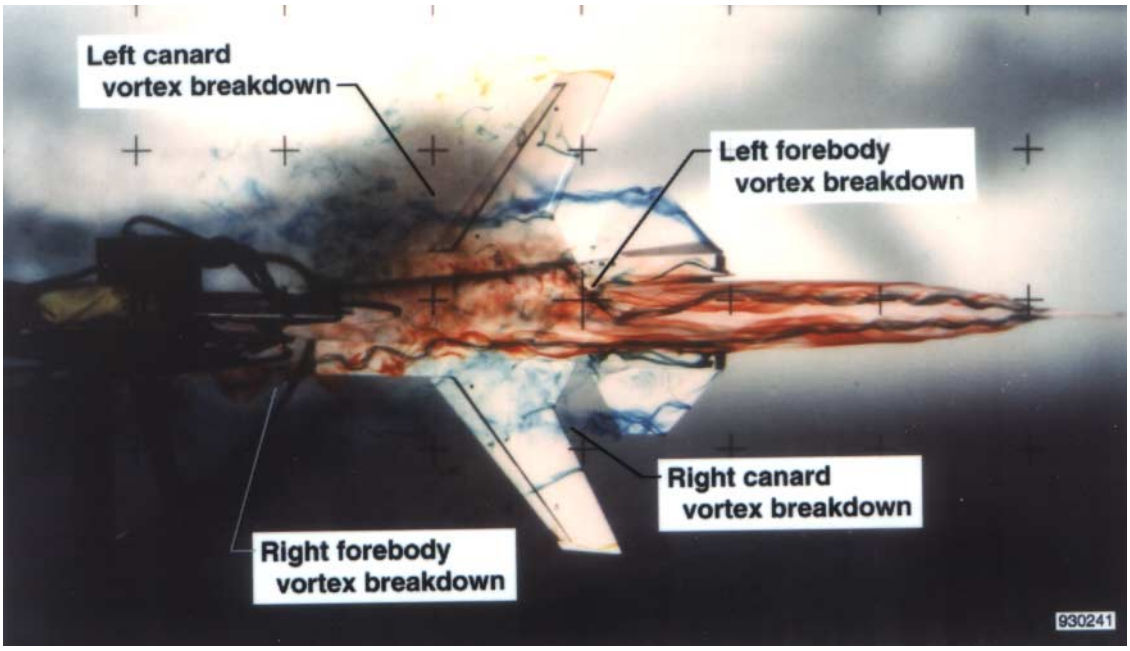

(a) Top view.

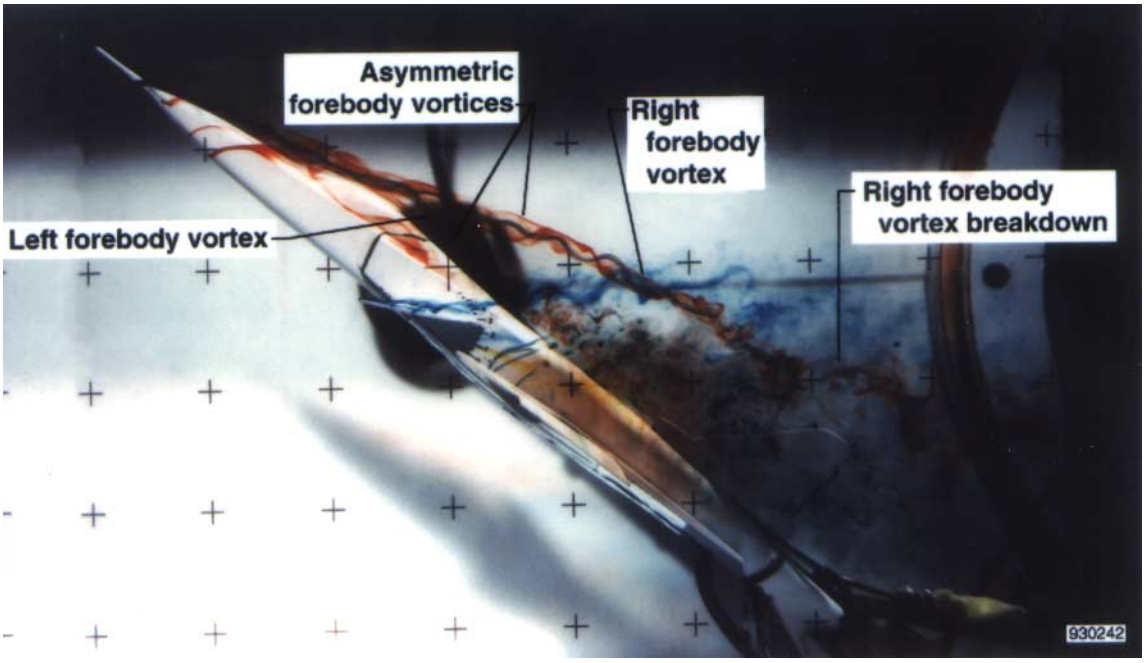

(b) Side view.

Figure 8. Characteristic flow patterns at $\alpha = 40°$ and $\beta = 0°$.

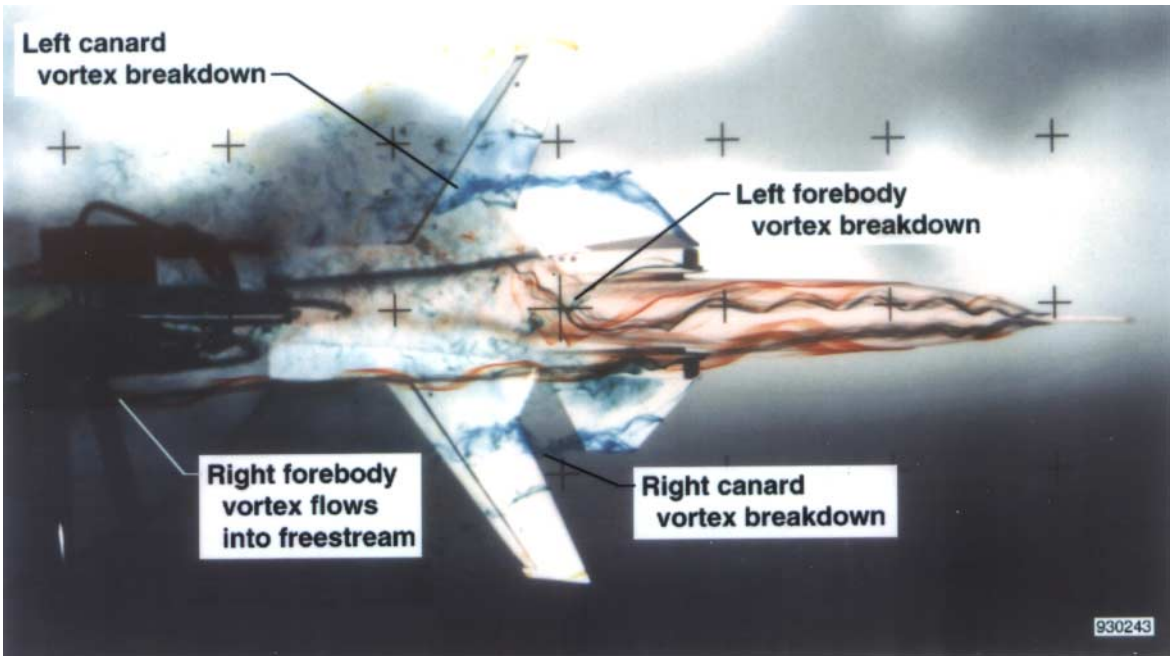

(a) Top view.

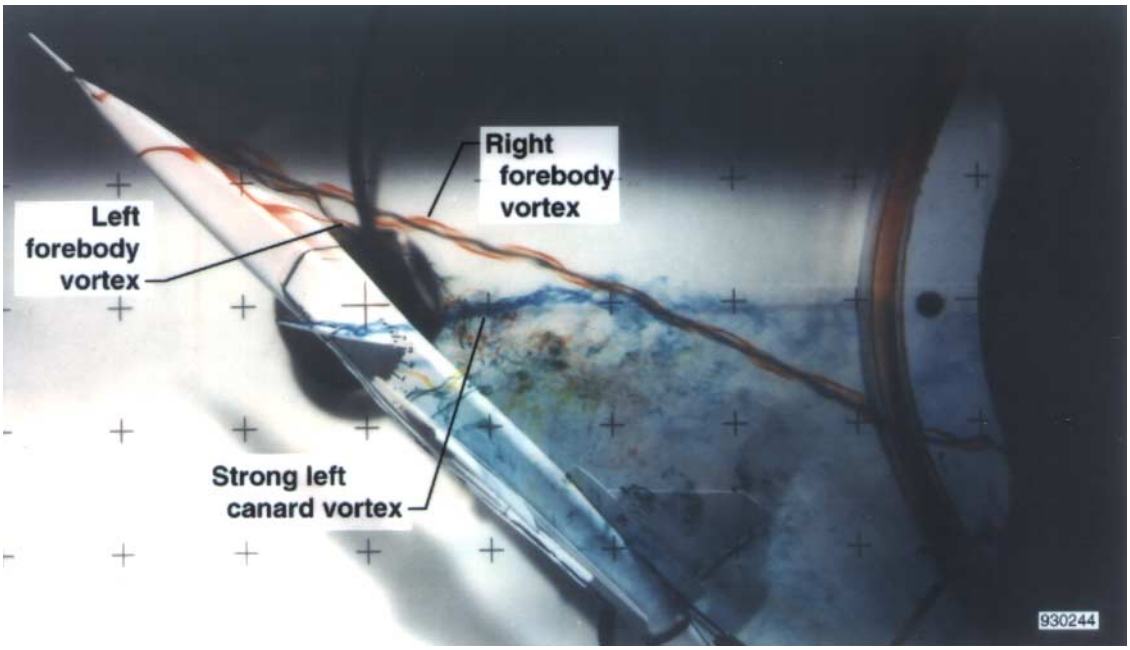

(b) Side view.

Figure 9. Characteristic flow patterns at $\alpha = 45°$ and $\beta = 0°$.

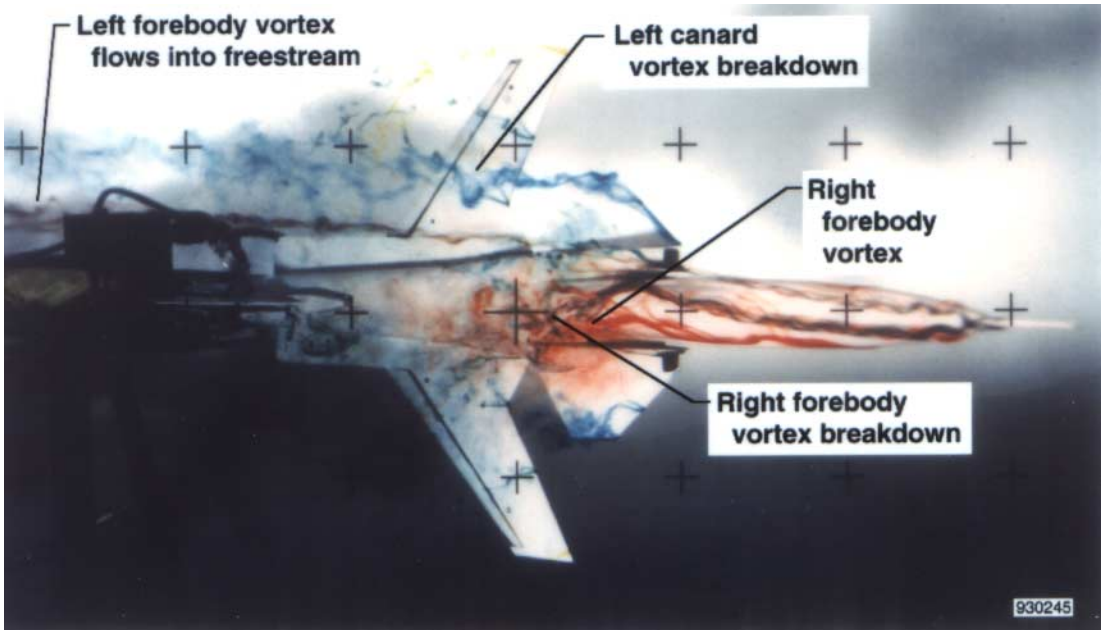

(a) Top view.

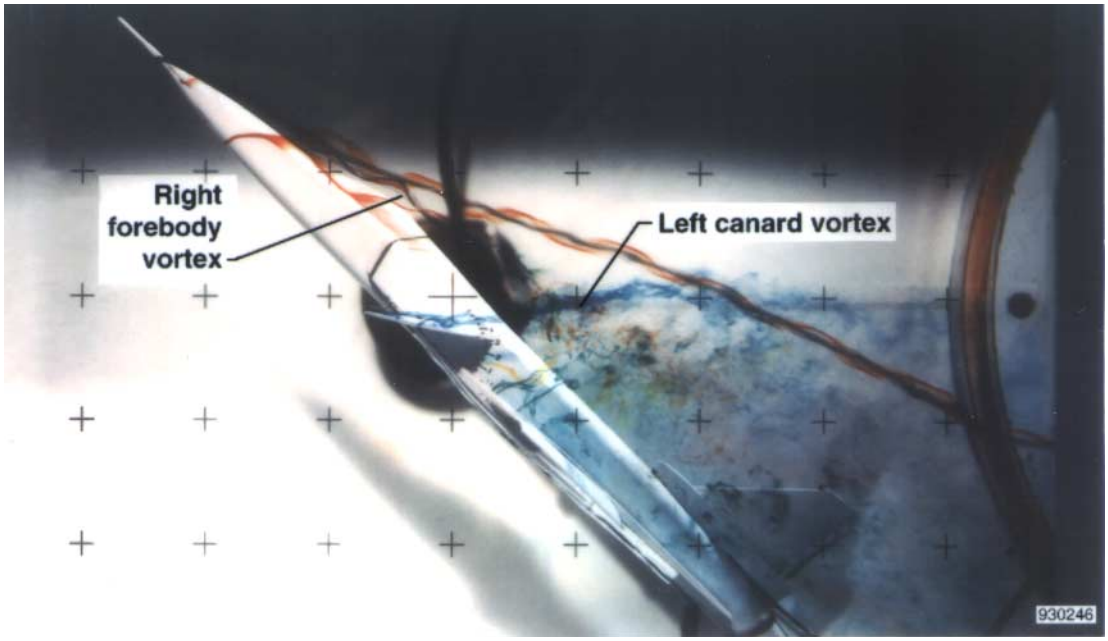

(b) Side view.

Figure 10. Characteristic flow patterns at $\alpha = 50°$ and $\beta = 0°$.

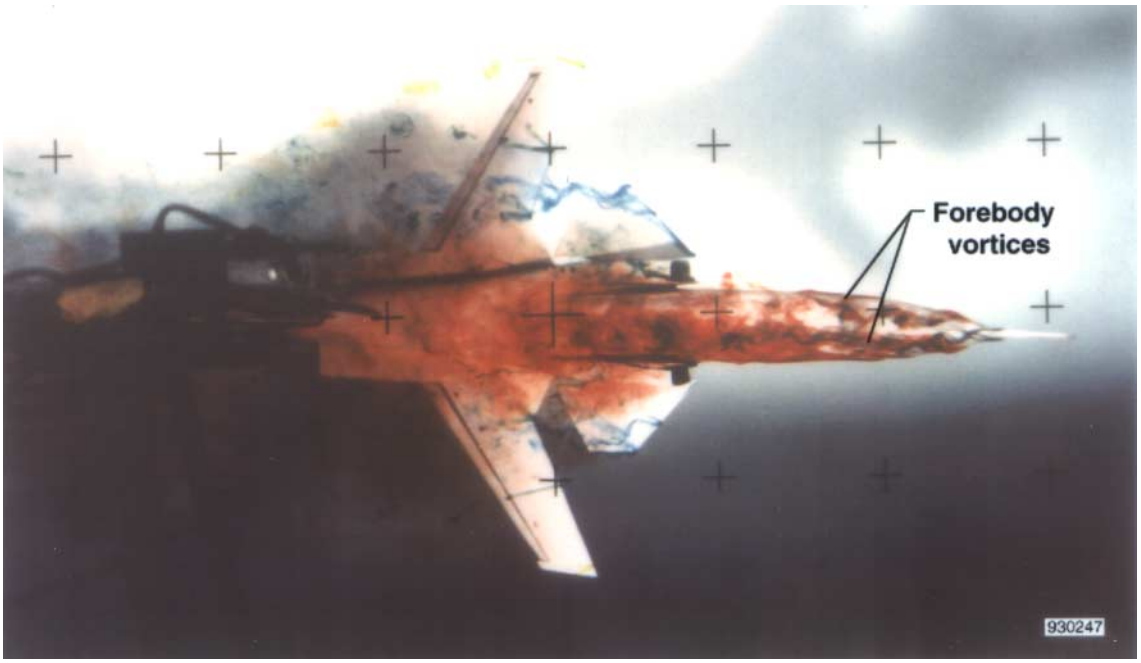

(a) Top view.

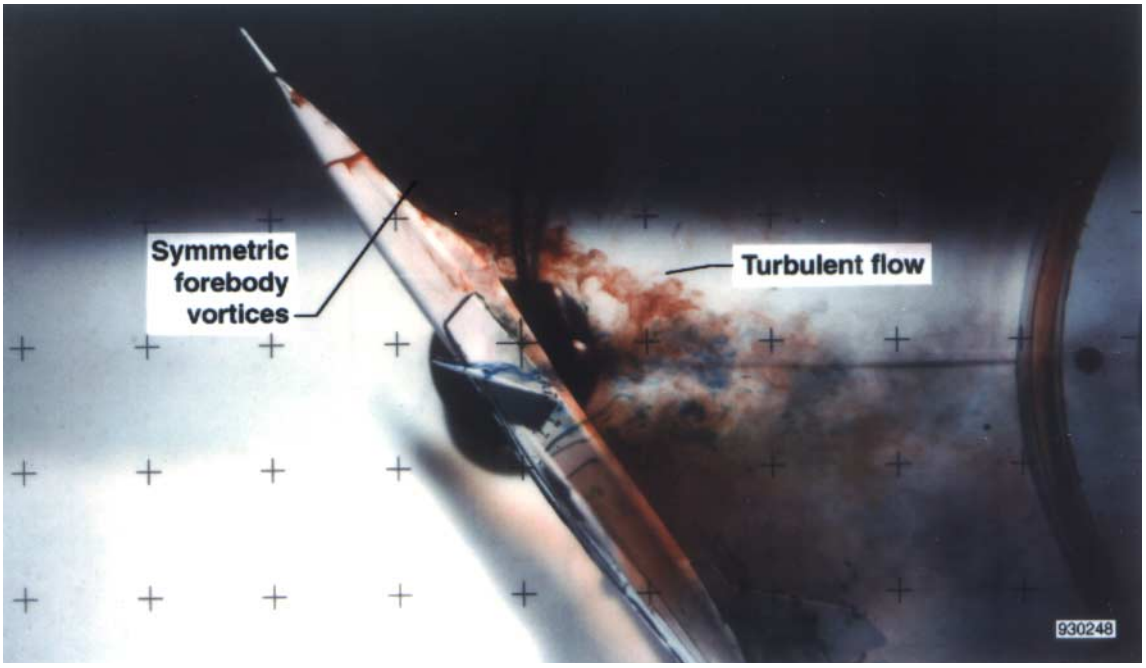

(b) Side view.

Figure 11. Characteristic flow patterns at $\alpha = 55°$ and $\beta = 0°$.

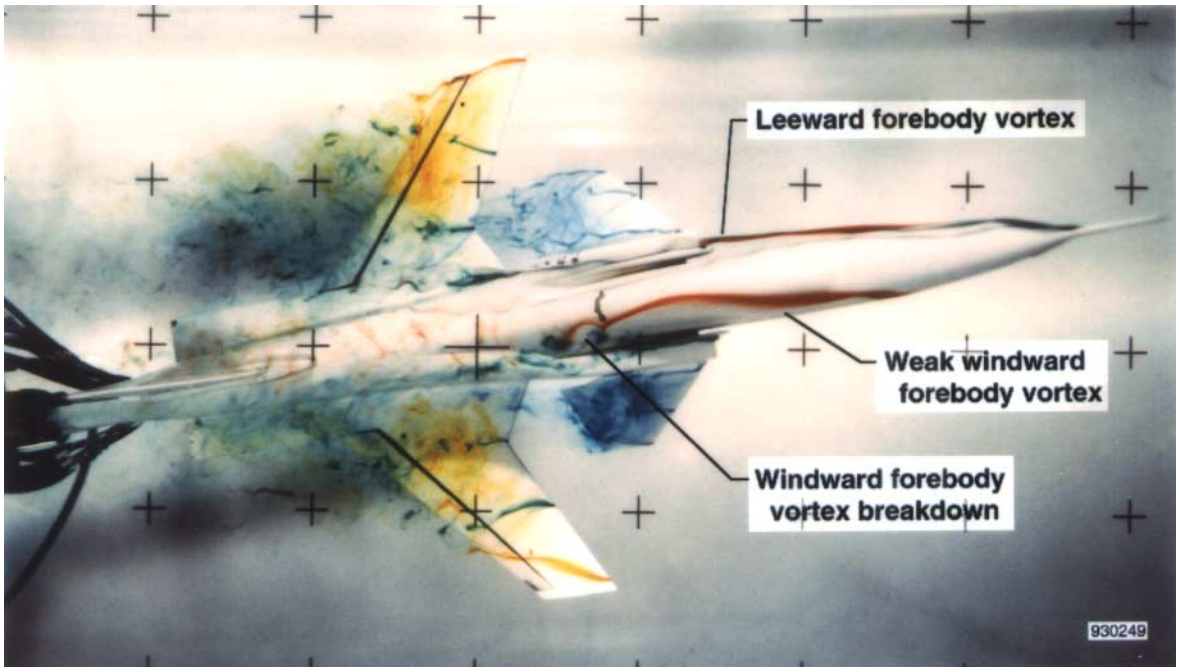

(a) Top view.

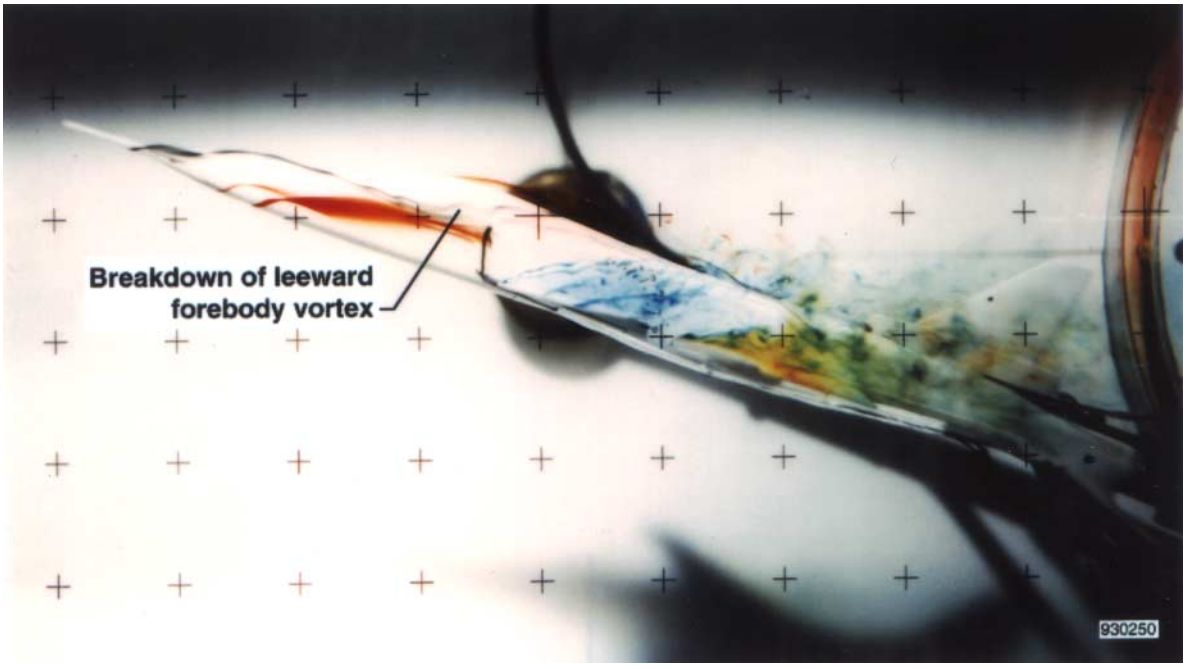

(b) Side view.

Figure 12. Characteristic flow patterns at $\alpha = 20°$ and $\beta = 5°$.

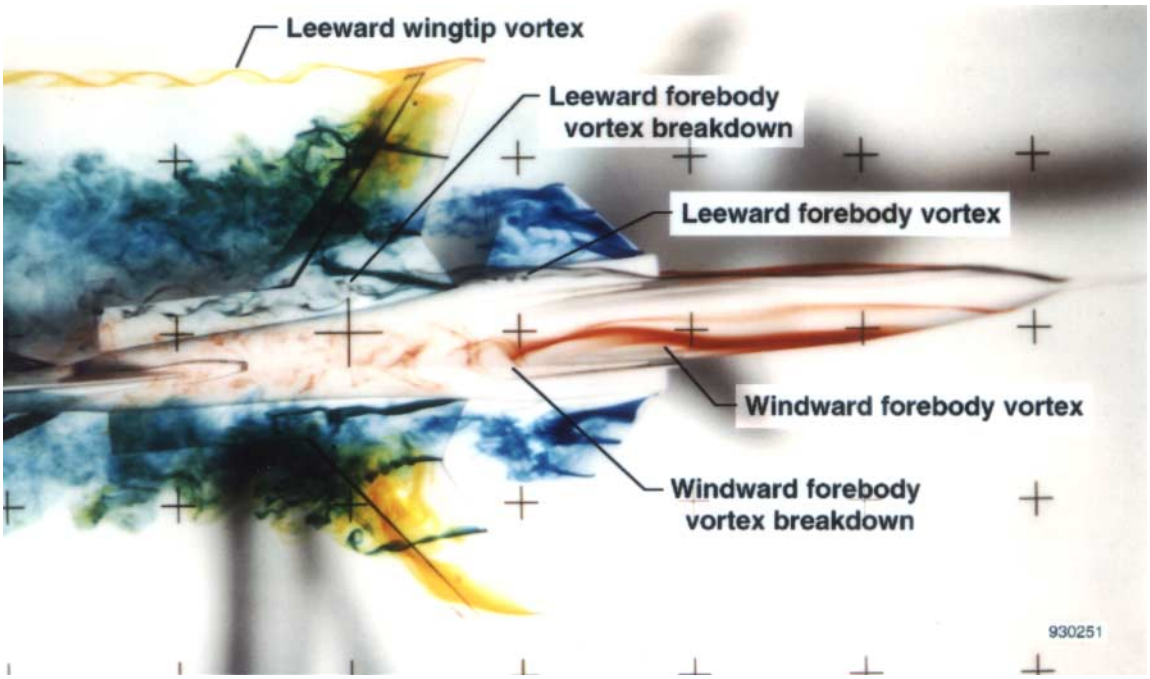

(a) Top view.

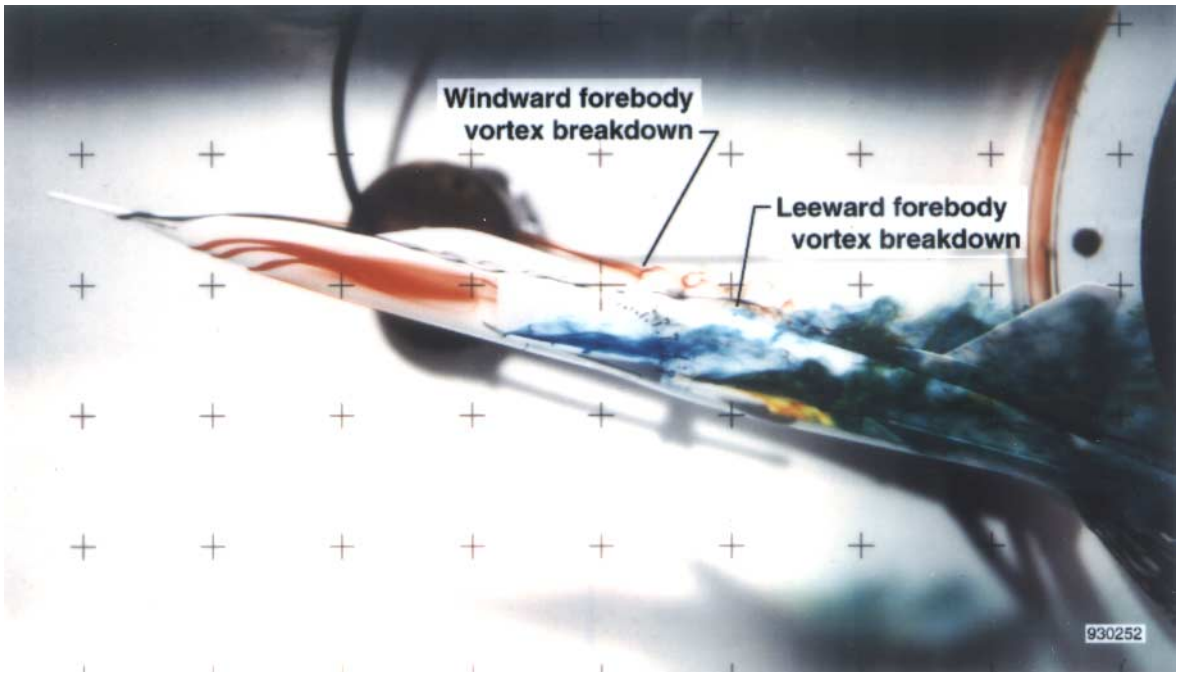

(b) Side view.

Figure 13. Characteristic flow patterns at $\alpha = 25°$ and $\beta = 5°$.

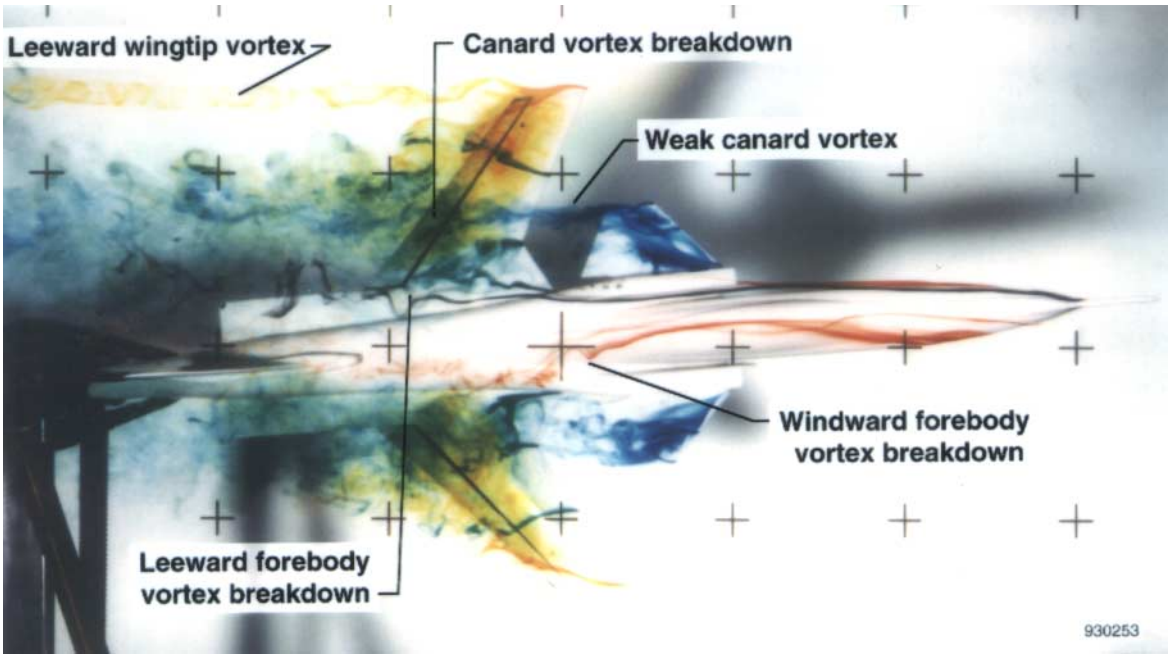

(a) Top view.

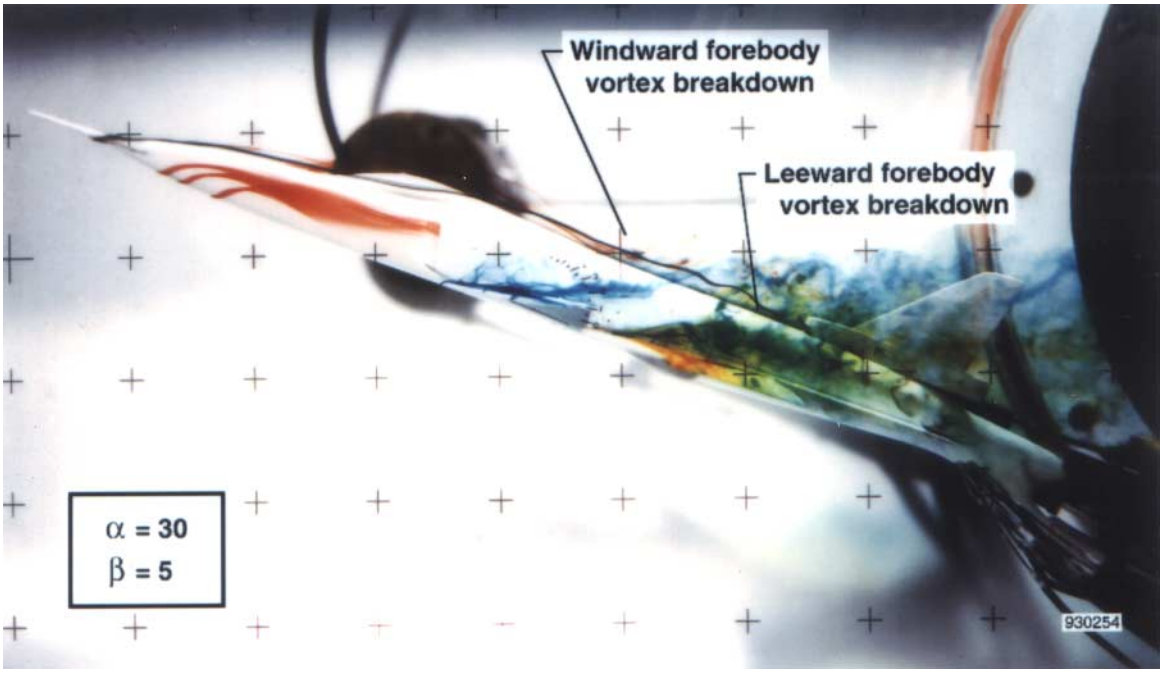

(b) Side view.

Figure 14. Characteristic flow patterns at $\alpha = 30°$ and $\beta = 5°$.

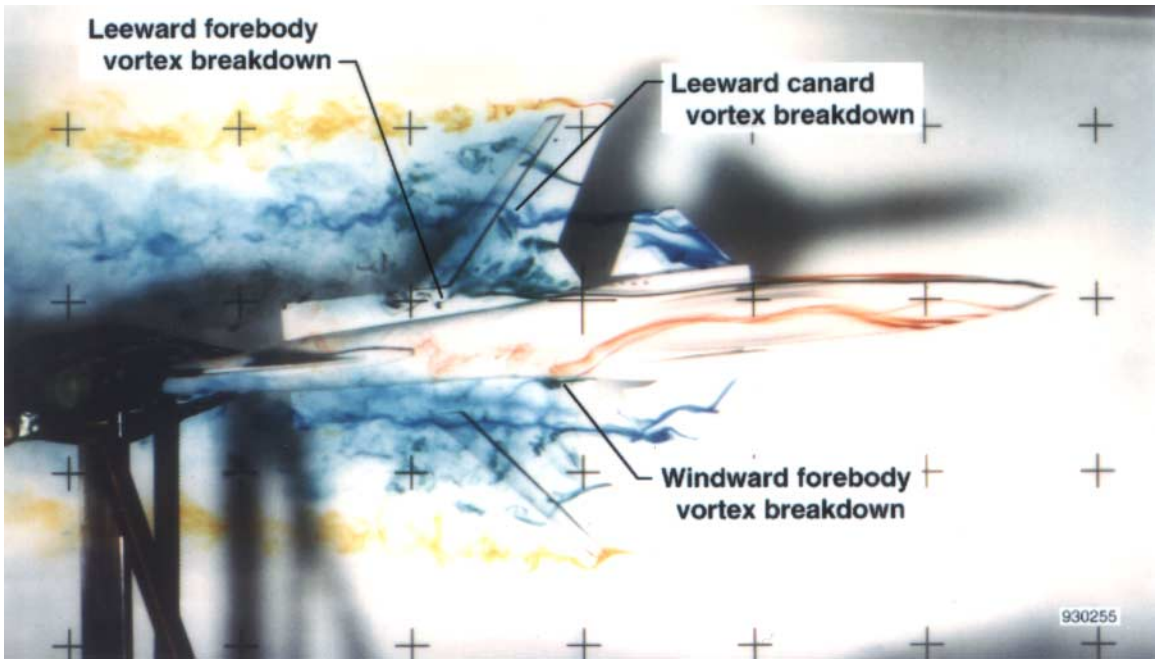

(a) Top view.

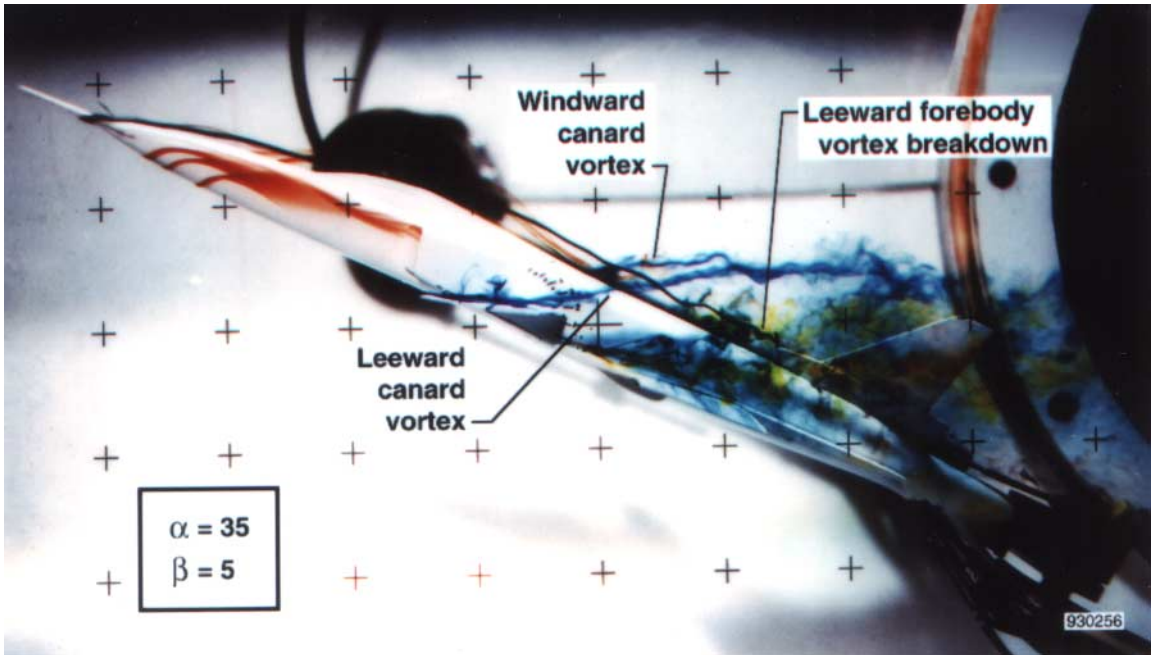

(b) Side view.

Figure 15. Characteristic flow patterns at $\alpha = 35°$ and $\beta = 5°$.

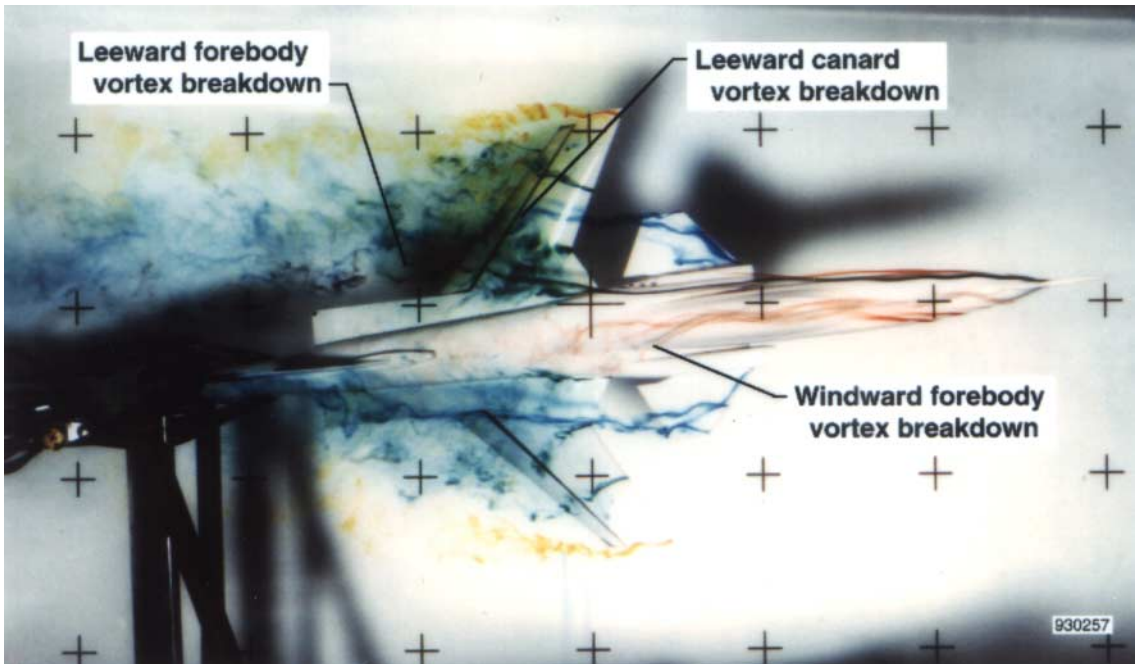

(a) Top view.

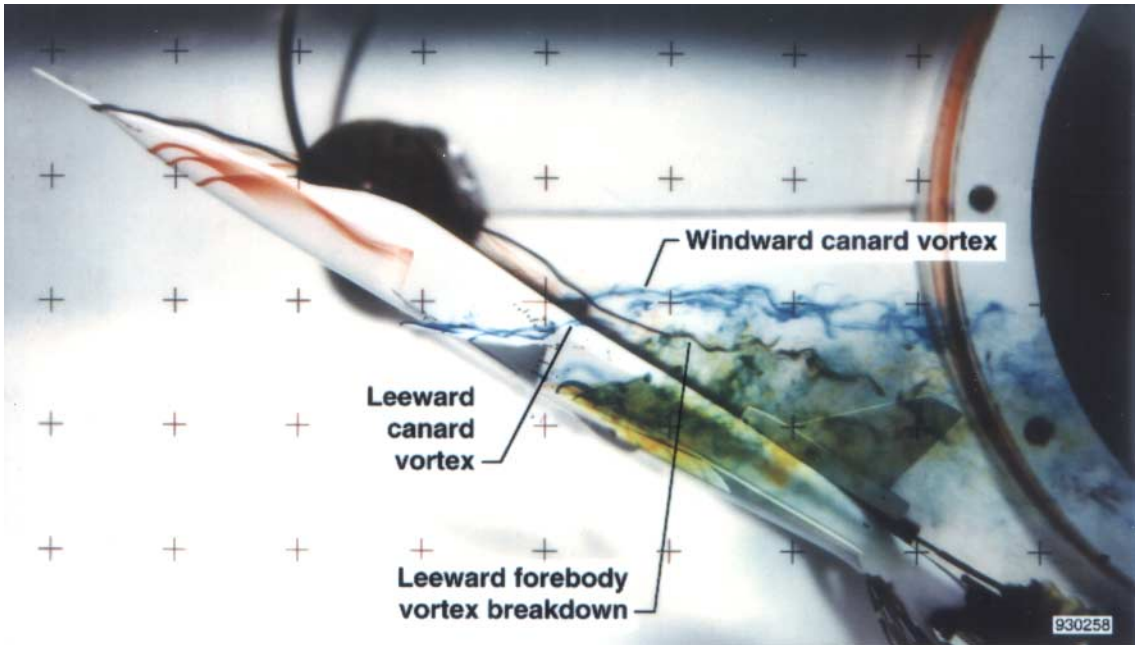

(b) Side view.

Figure 16. Characteristic flow patterns at $\alpha = 40°$ and $\beta = 5°$.

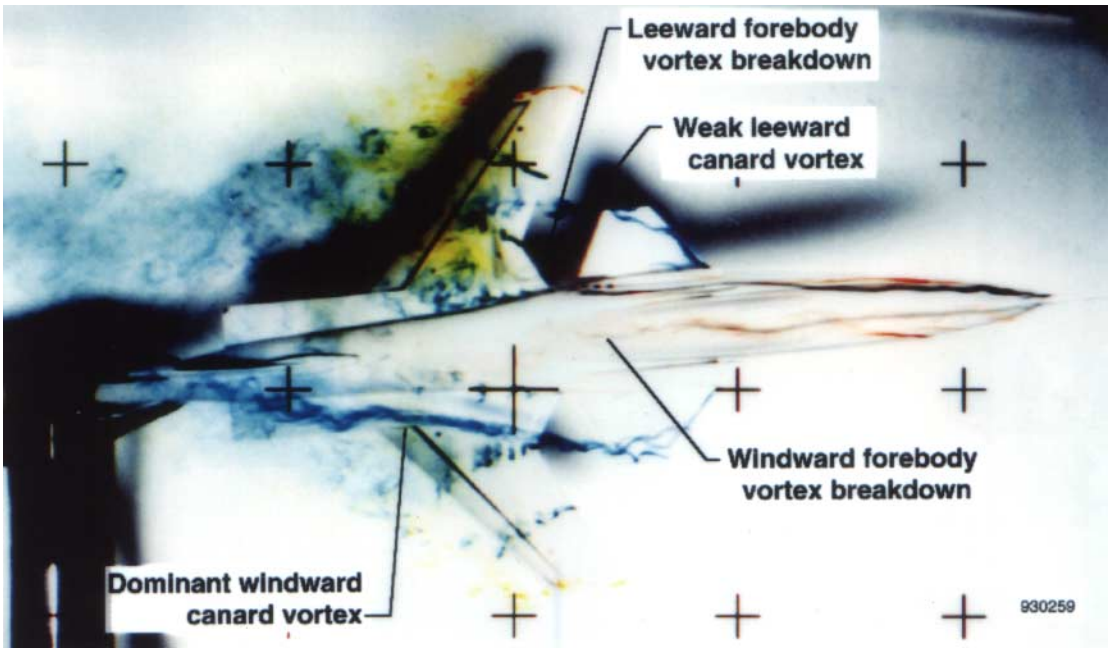

(a) Top view.

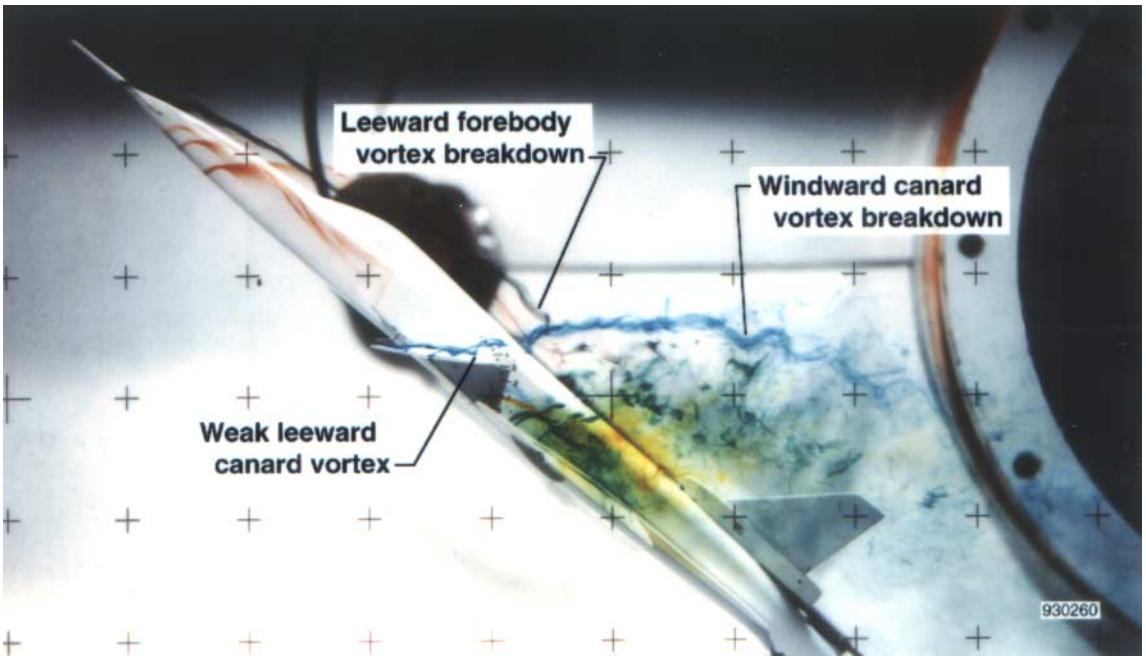

(b) Side view.

Figure 17. Characteristic flow patterns at $\alpha = 45°$ and $\beta = 5°$.

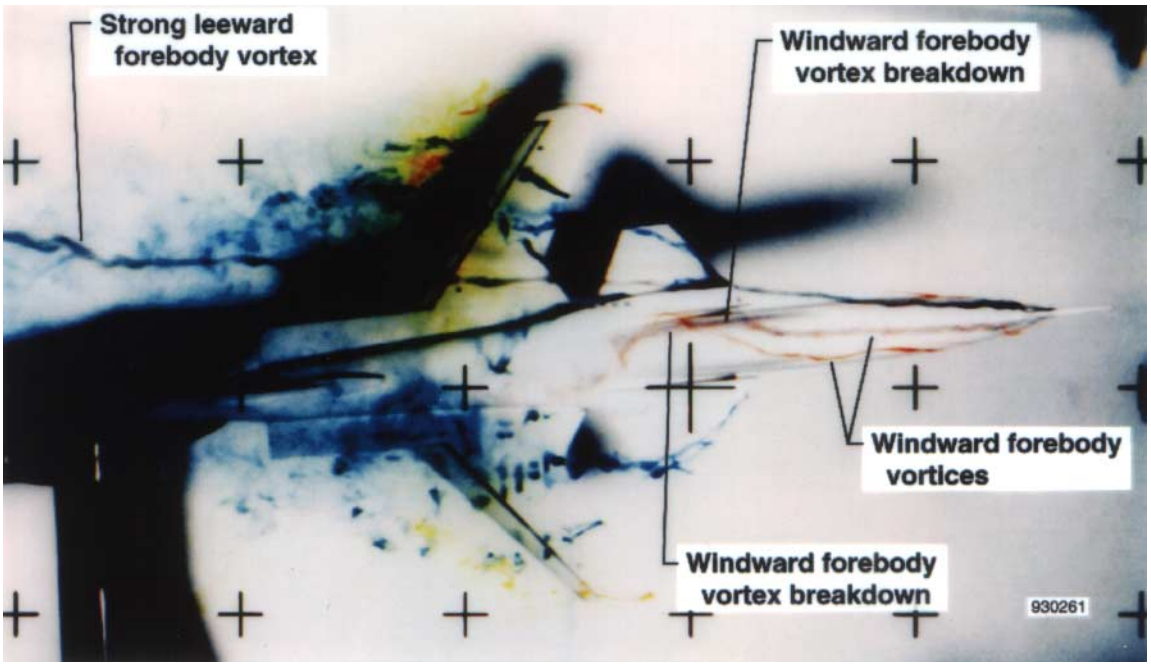

(a) Top view.

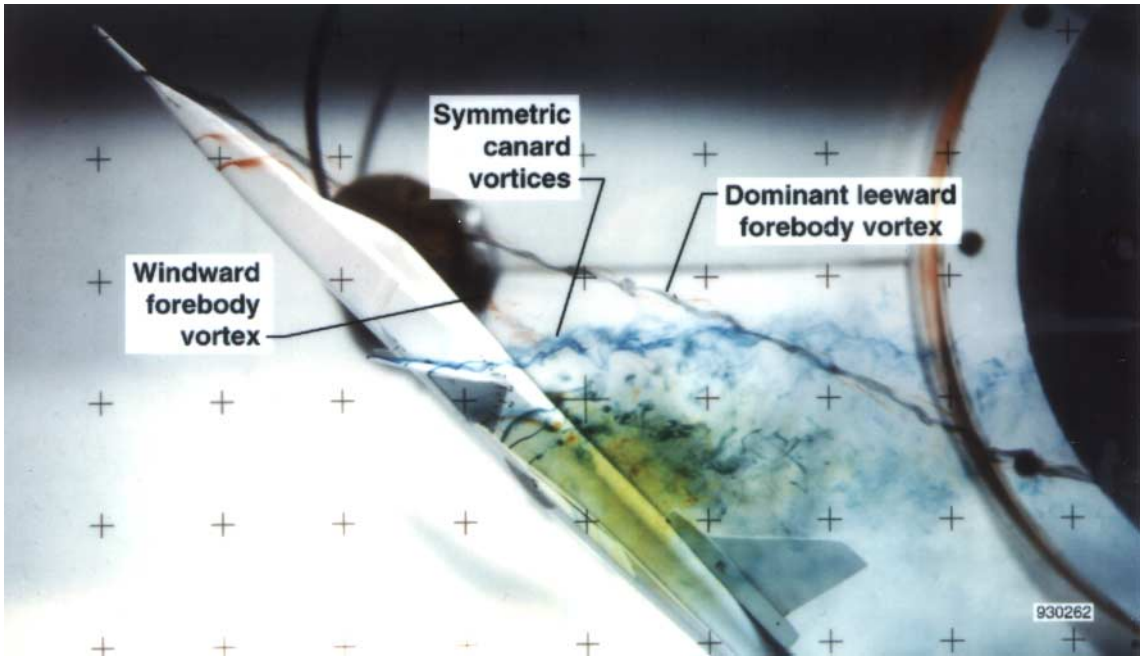

(b) Side view.

Figure 18. Characteristic flow patterns at $\alpha = 50°$ and $\beta = 5°$.

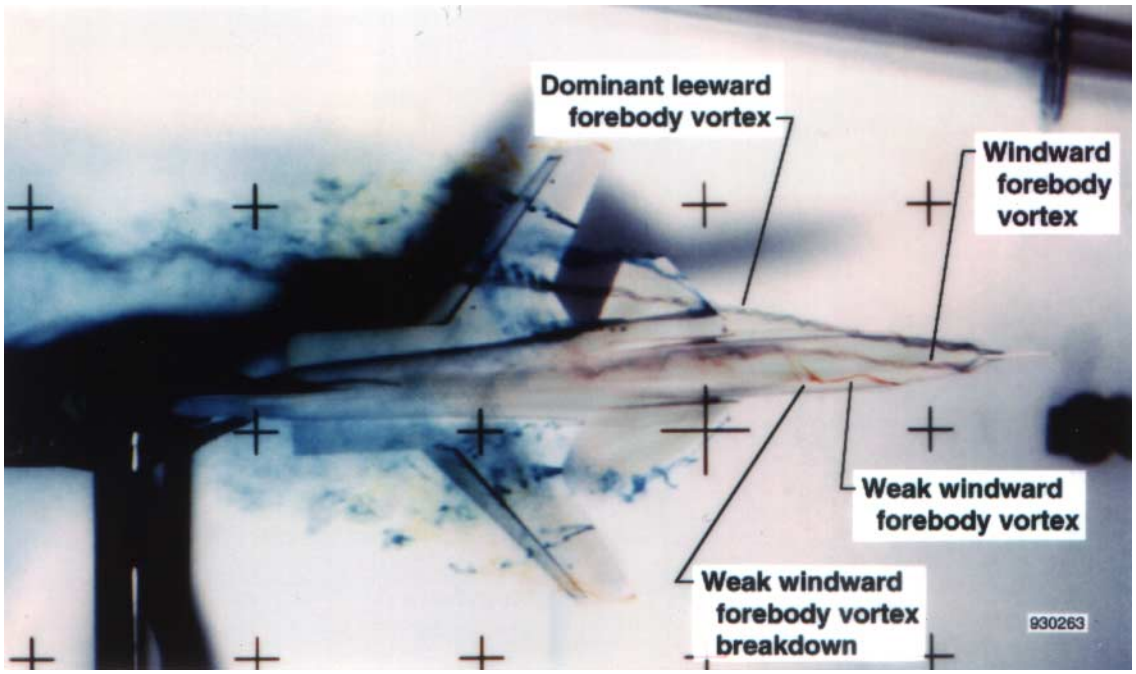

(a) Top view.

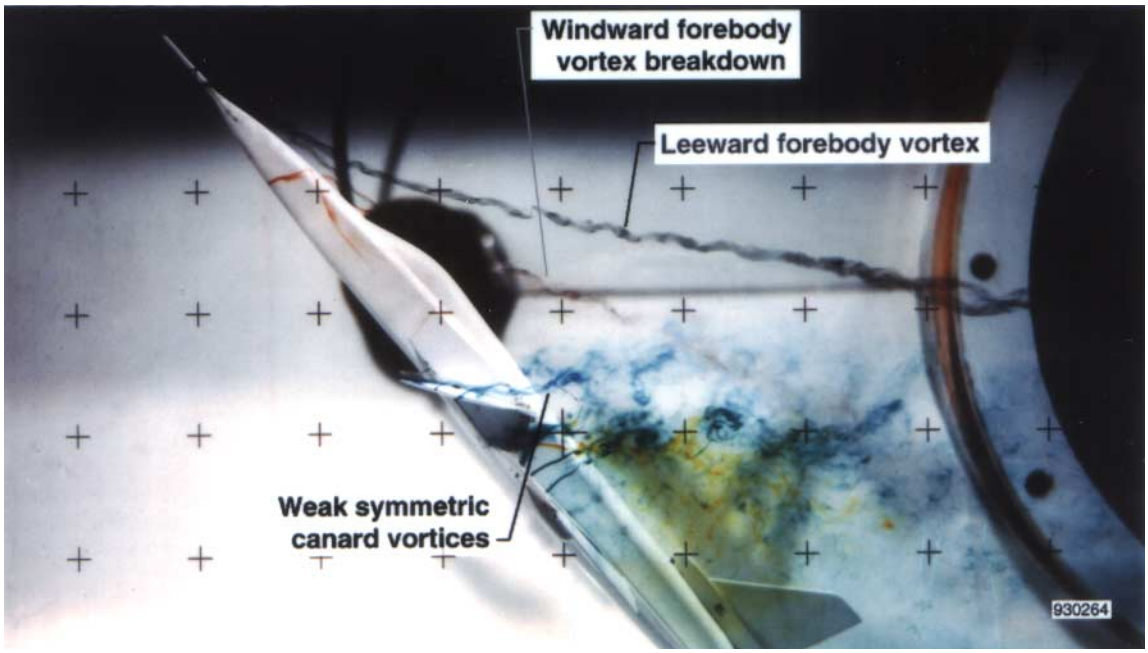

(b) Side view.

Figure 19. Characteristic flow patterns at $\alpha = 55°$ and $\beta = 5°$.

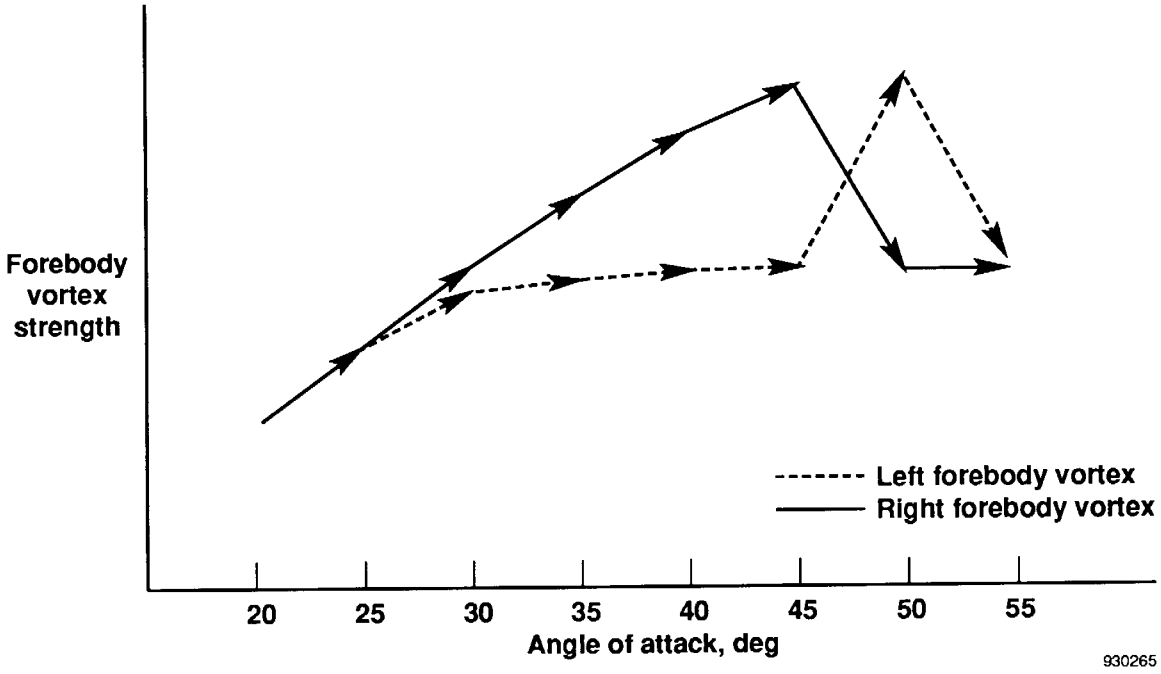

Figure 20. Effect of angle of attack on forebody vortex strength at $\beta = 0°$.

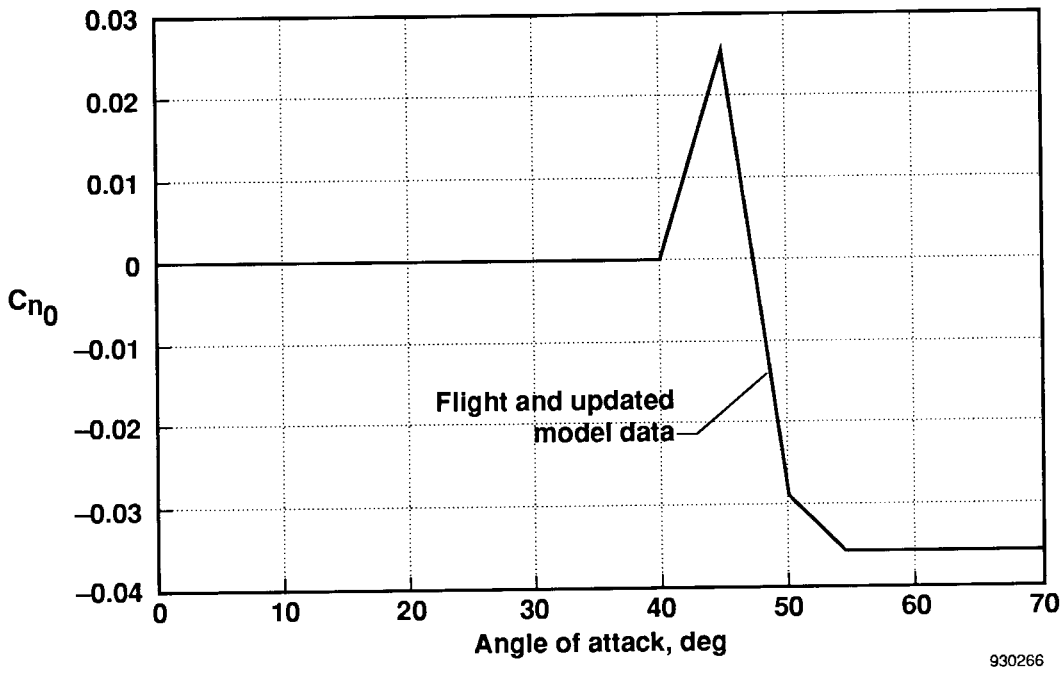

Figure 21. X-29A in-flight yaw asymmetries.

REPORT DOCUMENTATION PAGE

Form Approved
OMB No. 0704-0188

1. AGENCY USE ONLY (Leave blank)	2. REPORT DATE	3. REPORT TYPE AND DATES COVERED
	August 1994	Technical Memorandum

4. TITLE AND SUBTITLE

Flow-Visualization Study of the X-29A Aircraft at High Angle of Attack Using a 1/48-Scale Model

5. FUNDING NUMBERS

WU 533-02-38

6. AUTHOR(S)

Lt. Stacey J. Cotton (USAF) and Lisa J. Bjarke (NASA Dryden)

7. PERFORMING ORGANIZATION NAME(S) AND ADDRESS(ES)

NASA Dryden Flight Research Facility
P.O. Box 273
Edwards, California 93523-0273

8. PERFORMING ORGANIZATION REPORT NUMBER

H-1918

9. SPONSORING/MONITORING AGENCY NAME(S) AND ADDRESS(ES)

National Aeronautics and Space Administration
Washington, DC 20546-0001

10. SPONSORING/MONITORING AGENCY REPORT NUMBER

NASA TM-104268

11. SUPPLEMENTARY NOTES

12a. DISTRIBUTION/AVAILABILITY STATEMENT

Unclassified—Unlimited
Subject Category 02

12b. DISTRIBUTION CODE

13. ABSTRACT (Maximum 200 words)

A water-tunnel study on a 1/48-scale model of the X-29A aircraft was performed at the NASA Dryden Flow Visualization Facility. The water-tunnel test enhanced the results of the X-29A flight tests by providing flow-visualization data for comparison and insights into the aerodynamic characteristics of the aircraft. The model was placed in the water tunnel at angles of attack from 20° to 55° and with angles of sideslip from 0° to 5°. In general, flow-visualization techniques provided useful information on vortex formation, separation, and breakdown and their role in yaw asymmetries and tail buffeting. Asymmetric forebody vortices were observed at angles of attack greater than 30° with 0° sideslip and greater than 20° with 5° sideslip. While the asymmetric flows observed in the water tunnel did not agree fully with the flight data, they did show some of the same trends. In addition, the flow visualization indicated that the interaction of forebody vortices and the wing wake at angles of attack between 20° and 35° may cause vertical-tail buffeting observed in flight.

14. SUBJECT TERMS

Flow visualization, High angle of attack, Water tunnel, X-29A

15. NUMBER OF PAGES

50

16. PRICE CODE

AO3

17. SECURITY CLASSIFICATION OF REPORT	18. SECURITY CLASSIFICATION OF THIS PAGE	19. SECURITY CLASSIFICATION OF ABSTRACT	20. LIMITATION OF ABSTRACT
Unclassified	Unclassified	Unclassified	Unlimited

NSN 7540-01-280-5500

Available from the NASA Center for AeroSpace Information, 800 Elkridge Landing Road, Linthicum Heights, MD 21090; (301)621-0390

Standard Form 298 (Rev. 2-89)
Prescribed by ANSI Std. Z39-18
298-102